

ISTANBUL TECHNICAL UNIVERSITY ★ GRADUATE SCHOOL OF SCIENCE
ENGINEERING AND TECHNOLOGY

**MODELING THE LINKER MOVEMENT OF THE DYNEIN MOTOR
PROTEIN AT ATOMIC RESOLUTION**



M.Sc. THESIS

Mert GÖLCÜK

Department of Molecular Biology-Genetics & Biotechnology

Molecular Biology-Genetics & Biotechnology Programme

DECEMBER 2019

ISTANBUL TECHNICAL UNIVERSITY ★ GRADUATE SCHOOL OF SCIENCE
ENGINEERING AND TECHNOLOGY

**MODELING THE LINKER MOVEMENT OF THE DYNEIN MOTOR
PROTEIN AT ATOMIC RESOLUTION**



M.Sc. THESIS

Mert GÖLCÜK
(521181115)

Department of Molecular Biology-Genetics & Biotechnology

Molecular Biology-Genetics & Biotechnology Programme

Thesis Advisor: Assist. Prof. Mert Gür

İSTANBUL TEKNİK ÜNİVERSİTESİ ★ FEN BİLİMLERİ ENSTİTÜSÜ

**DİNEİN MOTOR PROTEİNİN KUVVET KOLU HAREKETİNİN ATOMİK
ÇÖZÜNÜRLÜKTE MODELLENMESİ.**

YÜKSEK LİSANS TEZİ

**Mert GÖLCÜK
(521181115)**

Moleküler Biyoloji-Genetik ve Biyoteknoloji Anabilim Dalı

Moleküler Biyoloji-Genetik ve Biyoteknoloji Programı

Tez Danışmanı: Dr. Öğr. Üyesi Mert GÜR





To society



FOREWORD

This thesis is written as a completion to the master degree of Molecular Biology-Genetics and Biotechnology at the Istanbul Technical University.

This study would not have been possible without the help of precious people.

I would like to express my sincere gratitude to Mert GÜR who has been always supportive and instructive to me, for providing the chance to study under his supervision. I would thank for his understanding, patience, and trust in me.

I appreciate all GURLAB members, Elhan TAKA, Sema Zeynep YILMAZ, Ceren KILINÇ, and Onur ÖZER especially for friendship, collaboration, sharing, strong support and patience.

I am thankful to all my close friends for their tolerance, support and the deepest discussions that shape my personality and mentality.

I would to express the most intense thanks to Ecem AYVAZ, for always being with me, for her love, support and patience.

Finally, I am deeply grateful to my family for their trust in me, love and support.

I would also like to acknowledge the financial support of TUBITAK for supporting my thesis with project no. 215Z398.

November 2019

Mert Gölcük



TABLE OF CONTENTS

	<u>Page</u>
FOREWORD	ix
TABLE OF CONTENTS	xi
ABBREVIATIONS	xiii
SYMBOLS	xv
LIST OF FIGURES	xvii
SUMMARY	xxi
ÖZET	xxiii
1. INTRODUCTION	1
1.1 Myosin.....	1
1.2 Kinesin	2
1.3 Dynein	2
1.3.1 Dynein structure	3
1.3.2 Dynein mechanochemical cycle.....	4
1.3.3 Linker	6
2. METHODOLOGY	9
2.1 MD Simulation Details.....	9
2.2 Modelling the Linker Movement of Dynein with Steered MD Simulations....	10
2.2.1 Theory	10
2.2.2 Selection of SMD simulation parameters	11
2.3 Modelling the Linker Movement with Targeted MD Simulations.....	14
2.3.1 Theory	14
2.4 Umbrella Sampling and Weighted Histogram Method for Free-Energy Calculations.....	14
2.5 Covariance Matrix and Principle Component Analysis.....	17
3. RESULTS & DISCUSSION	19
3.1 Selection of SMD Parameters	19
3.2 Modelling the Linker Priming Stroke Reveals Steric Clash Between the Linker and AAA4	21
3.3 The Linker Movement During Priming Stroke is Energetically Favorable	23
3.4 Principal Component Analysis	23
3.5 Free Energy Surface Calculation.....	24
3.6 During Priming Stroke the Linker Interdomain Salt Bridges Switch from AAA4 to AAA3	26
4. CONCLUSION AND FUTURE RESEARCH	29
REFERENCES	31
APPENDICES	37
Appendix A: Sequence alignment of the Dynein.....	27
CURRICULUM VITAE	43



ABBREVIATIONS

ATP: Adenosine Tri-Phosphate

MT: Microtubule

AAA+: ATPases Associated with diverse cellular Activities

ER: Endoplasmic Reticulum

ALS: Amyotrophic Lateral Sclerosis

DHC: Dynein Heavy Chain

MTBD: Microtubule Binding Domain

P-loop: Phosphate binding loop

NAMD: Nanoscale Molecular Dynamics

VMD: Visual Molecular Dynamics

PME: Particle-Mesh Ewald

vdW: van der Waals

MD: Molecular Dynamics

SMD: Steered Molecular Dynamics

TMD: Targeted Molecular Dynamics

CMD: Constrained Molecular Dynamics



SYMBOLS

C	: Covariance matrix
F	: Force
k	: Spring constant
n	: Direction of pulling
N	: Total number of atoms
P	: Pressure
R	: Universal gas constant
R	: Coordinate
t	: Time
T	: Temperature
TS	: Thermodynamic State
U	: Potential energy
v	: Pulling velocity
ξ	: Reaction coordinate
σ	: Variance
$U^{(b)}$: Biased potential
$U^{(u)}$: Unbiased potential
Å	: Ångstrom



LIST OF FIGURES

Page

- Figure 1.1 :** Schematic representation of Dynein and Linker. A) Illustrative representation of cytoplasmic dynein domains linker, AAA+ ring, buttress, stalk and MTBD. B) Crystal structure of the cytoplasmic dynein (PDB ID 4RH7 (Schmidt, Zalyte, Urnavicius, & Carter, 2015)) shown in surface representation using the same color selection as in A). On the right hand side, the static region of the linker (H11-H18) is shown in a darker tone of magenta while the rigid-body moving region of the linker (H5-H9) is shown in a lighter tone. Hinge helix (H10) is shown in violet. 4
- Figure 1.2 :** Mechanochemical cycle of the dynein. The AAA+ ring is composed of six AAA domains and binds to MTs through a coiled-coil stalk with a small MTBD. The linker undergoes ATP dependent conformational changes and generates force and motility, synchronized with MT binding/unbinding cycles. 6
- Figure 2.1 :** Alignment of the cytoplasmic dynein linker in bent conformation (PDB: 4RH7) with straight conformation (PDB: 3VKG). A) Linker bent conformation (Purple) and straight conformation (transparent grey). Orange color indicated residues are SMD atoms, green color indicated residues are aligned atoms, and cyan colored atoms are fixed atoms. B) Sequence alignment is performed for two structures and sequences of the alpha helices and beta sheets are shown in the alignment. 13
- Figure 3.1 :** Spring constant selection for the SMD simulations. Second trial of SMD simulations for the pulling velocity of 1 \AA/ns was selected. And, spring constants of 10, 25, 50, 75, and $100 \text{ kcal/mol/\AA}^2$ parameters; SMD atoms were the C^α atoms of the L1264, L1309, and V1325 residues, and fixed atoms were the C^α atoms of L1415-A1425 residues. Blue lines indicates displacement of the SMD atoms and red line indicates the displacement of dummy atom. 19
- Figure 3.2 :** Structural deformations. Initial structure of the linker shown in blue and structure obtained from 5th SMD simulation shown in pink. In the red circle shown on the left, a structural shift was observed in the hinge region compared to the initial structure. In the red circle shown on the right, structural disruptions in the alpha helices of linker is observed, while it is expected to be rigid. 20
- Figure 3.3 :** Spring constant selection for the SMD simulations. Second trial of SMD simulations for the pulling velocity of 1 \AA/ns was selected. And, spring constants of 10, 25, 50, 75, and $100 \text{ kcal/mol/\AA}^2$ parameters; SMD atoms were the C^α atoms of G1256-G1271 (H4), K1296-K1313 (H5), and E1322-W1349 (H7) residues, and fixed atoms were the C^α atoms of L1415-A1424 (H10-hinge) and D1434-G1442 (H12) residues. Blue lines

- indicates displacement of the SMD atoms and red line indicates the displacement of dummy atom. 21
- Figure 3.4 :** Progress of SMD simulation protocol towards the target linker structure. A) Movement of the center of mass of the pulled atom along the trajectories of SMD and CMD simulations. Blue lines represent the SMD simulations and red lines represent the CMD simulations. B) Change in the RMSD according to the target linker structure in TS1 (3VKG). Blue lines represent the SMD simulations and red lines represent the CMD simulations. The line on the 80. ns points out that the values after there won't be used. 22
- Figure 3.5 :** Steric clash between the Link1-2 region of linker and AAA4L site. Left panel shows the AAA+ ring of the dynein obtained conformations after 80 ns of SMD-CMD simulations. Linker and AAA4, which are involved in the steric clash, are shown in cartoon representation whereas the remaining the remaining structural components are shown in surface representation. Right top panel shows the steric clash taking place between linker helices (H5-H7 and H10) and PS-I insert of AAA4L site. The right bottom panel shows the schematic illustration of the dynein AAA+ ring and linker during the steric clash. Large (L) and small (S) subdomains of AAA+ domains are shown separately in the schematic representation. 22
- Figure 3.6 :** Distribution of UMD simulations along the ξ . Dashed line indicates the gates, and yellow stars indicates center positions of the UMD. 23
- Figure 3.7 :** Principal Component Analysis of UMD simulations. (A-B) The first two principal components of the complete UMD simulations data superimposed on a (TS3*: ATP, β , pre) conformation is shown. (C) Distribution of UMD simulations conformers along the first two principal components are shown. Dashed lines indicate the approximate position of the reaction coordinate on the distribution. (TS3: ADP.Pi, β , pre) and (TS5: ADP, α , post) crystal structures are shown with grey and magenta squares, respectively. 24
- Figure 3.8 :** Free energy profile along the reaction coordinate with error bar of the linker priming movement. Free energy profile as a function of the RMSD between the extended linker structure and the linker conformations sampled during UMD simulations. 25
- Figure 3.9 :** Free energy profile error estimation with Bootstrapping analysis. In this graph show that PMF construct from randomly sampled values according to the obtained weighted histograms. 25
- Figure 3.10 :** Location of salt bridges broken and formed throughout the linker movement during priming stroke. (A) Type II interdomain salt bridges between Link1-2 and AAA3-4 of the straight linker are shown. (B) The type 2 interdomain salt bridge with AAA3 and the intradomain salt bridges of the bent linker are shown. (C) Salt bridges in the left panels are numbered and each salt bridge is magnified in the right panel. 26
- Figure 3.11 :** Evolution of salt bridges during the linker movement of the priming stroke (A) Illustrative representation of the linker position with respect to the AAA+ ring along the reaction coordinate. (B) Representative conformations sampled from UMD simulations along the reaction coordinate. (C) Presence of Type II salt bridges along the reaction coordinate. White colors indicate that the salt bridges are not present at

that specific point along the reaction coordinate. The coloring for the salt bridge indicates the domain with which Link1-2 is forming a salt bridge. Thus, magenta indicates intradomain salt bridges. Green and yellow indicate interdomain salt bridges between the linker and AAA3 and AAA4, respectively..... 28





MODELING THE LINKER MOVEMENT OF THE DYNEIN MOTOR PROTEIN AT ATOMIC RESOLUTION

SUMMARY

Eukaryotic cells are required intracellular order to perform fundamental activities. Intracellular organization of the eukaryotic cells are provided by cytoskeletal motor proteins moving across the cytosolic tracks, which are microtubules (MT) and actin filaments, by hydrolyzing Adenosine Triphosphate (ATP). These motor proteins take crucial roles in the eukaryotic cells, such as ciliary beating, muscle contractions, cell divisions, vesicular transport, and neuronal development and transportation.

Cytoskeletal motor proteins are differ in their structure, movement direction, cytosolic tracks that they bind, and the cargos that they carry. These motor proteins are divided in three families; kinesin, dynein, and myosin families. Members of kinesin and dynein families move along the MT, whereas myosin family members move along the actin filaments. Kinesin protein family comprises members moving to plus (+) or minus (-) end of the MT. Myosin family member motor proteins move either to barbed (+) or pointed (-) end of the actin filaments. Dynein motor proteins, on the other hand, move towards to minus end of the MT.

Cytoplasmic dynein interacts with many intracellular pathways. Dyneins carry aggregated proteins, transcription factors mRNA containing particles, viruses, membrane-bound organelles, phagosomes, vesicles moving from the endoplasmic reticulum (ER) to Golgi, lipid droplets, lysosomes, melanosomes, peroxisomes, mitochondria, and endosomes. In neurons, dynein drives retrograde transport towards the cell body and is required for neuronal migration, growth, and synapse formation. Numerous neurodegenerative diseases, including amyotrophic lateral sclerosis, Charcot-Marie-Tooth, Alzheimer's, Parkinson's and Huntington's, lissencephaly and ciliary dyskinesia. This close relationship necessitates; especially if new therapeutic strategies are considered; understanding the operation of dynein and functional malfunctions causing those diseases. Dynein also plays important roles in cell division, such as maintenance of the proper tension and length of the spindle, focusing MTs into spindle poles, and regulation of the spindle assembly checkpoint activation and proper chromosome segregation.

Understanding how dynein generates motility and force on MTs is essential to develop novel chemical inhibitors/modifiers of dynein function for the treatment. Cytoplasmic dynein is composed of two identical dynein heavy chains (DHCs) and several smaller associated polypeptides. DHC contains a C-terminal motor domain (head) and an N-terminal tail domain. The head contains six AAA modules (AAA1-AAA6) organized into a hexameric ring. ATP hydrolysis occurs in AAA1-AAA4 domains, where AAA1 is the main ATP site and necessary for motility. In addition to the AAA+ domain, dynein also contains the linker, the stalk, the buttress, and the C-terminal domain. ATP binding and beginning hydrolysis results in a conformational change of the linker from

a straight conformation to a bent conformation. This conformational change is referred to as the priming stroke. Upon microtubule binding, the power stroke of dynein takes place during which the linker returns to a straight conformation. To the best of our knowledge, all-atom Molecular Dynamics (MD) simulations of the linker movement during the priming and power stroke have not been performed in the literature. Moreover, the energetics and structural mechanism remains to be elucidated. For the full-length dynein motor domain, only a very limited number of all-atom MD simulations studies exists in the literature. Recently, MD simulations of human dynein-2 in its pre-power stroke state in the presence of explicit water and ions was performed in the literature. Using the solvated and equilibrated full-length motor domain conformation of this study (~800,000 atoms in size), an extensive set of new MD simulations totaling 500ns in length were performed. In these MD simulations, the linker domain is guided towards its post-power stroke structure and free energy surface along the transition is constructed. As a first step, an initial transition path of the dynein linker was constructed by using a combination of steered MD (SMD) simulations and constrained MD simulations. As a result of SMD simulations, conformations were sampled along the linker transition pathway and the steric clash due to the contact between the linker and the AAA4 were observed. Subsequently, umbrella sampling MD (UMD) simulations were performed. UMD simulations were performed to extensively sample the transition pathway and explore the energetics of the linker conformational transition. RMSD of the linker to its straight conformation was selected as the reaction coordinate ξ . Weighted Histogram Analysis Method (WHAM) was applied using the UMD simulations data. And the free energy surface as a function of ξ was constructed. Free energy difference between of the bent and the straight conformations of the dynein linker was obtained ~ -40 kJ/mol. Thus, indicating that linker movement during the priming stroke is energetically favorable. All UMD simulations were combined into a single trajectory and principal component analysis were performed to investigate main features of the linker transition. Distribution of inter and intra domain salt bridge of the linker were investigated along the transition pathway. 9 salt bridges forming or breaking during the linker transition were identified. Among them 6 salt bridges were present in the straight conformation while 3 were present in the bent conformation.

DİNEİN KUVVET KOLUNUN HAREKETİNİN ATOMİK ÇÖZÜNÜRLÜKTE MODELLENMESİ.

ÖZET

Ökaryotik hücrelerin sağlıklı bir şekilde çalışabilmesi için hücre içi ulaşım ve organizasyon son derece önemlidir. Hücre içi ulaşım ve organizasyon, hücrenin mikrotübülleri (MT'leri) ve aktin filamentleri üzerinde yürüyen motor protein aileleri tarafından gerçekleştirilir. Motor protein ailelerinin yapılarında, bağlandıkları sitozolik yollarda, sitozolik yollar üzerindeki hareket doğrultularında ve taşıdıkları kargolarda farklılıklar bulunmaktadır. Motor proteinleri üç aileye ayrılmaktadır; miyozinler, kinezinler ve dineinler. Miyozinler, aktin filamentleri üzerinde + veya – uca doğru hareket edebilirler. Benzer şekilde, kinezinler de MT'ler üzerinde + veya – yöne doğru hareket edebilirler. Dineinler ise MT'ler üzerinde – yöne doğru hareket ederler.

Miyozin ailesi birçok alt aileye sahiptir. Miyozinler, farklı hücre tiplerinde ve organlarda bulunabilirler. Miyozin ailesinin genel olarak yapıları incelendiğinde 1000-2000 amino asit uzunluğunda oldukları görülmektedir. Bu yapılar 3 bölgeye ayrılır; evrimsel olarak korunmuş olan baş yapısı ATPaz aktivitesine sahip olup myozinlerin hareketinden ve aktinlere bağlanmasından sorumludur, boyun bölgesi ise baş bölgesi ile kuyruk bölgesini bağlar. Ayrıca, düzenleyici proteinlerin bağlanması için bir bölgedir. Bu bölge hafif zincir bölgesi olarak adlandırılır, kuyruk yapısı ise yüklerin bağlanması ve myozinlerin dimerizasyon ve oligomerizasyonlarından sorumludur.

Dineinler, AAA + (çeşitli hücresel Aktiviteler ile İlişkili ATPazlar) ailesinin üyesidir ve genellikle iki ana alt aileye ayrılır: aksonemal ve sitoplazmik dynein. Aksonemal dinein alt ailesi, flagella ve silianın vuruş hareketinden sorumludur. Sitoplazmik dinein alt familyası ise, taşıma, yönlendirilmiş hücre hareketi, mitoz bölünme ve hücre polarizasyonundan sorumludur

Sitoplazmik dinein hücre içindeki birçok yolla etkileşime girer. Dineinler, kümelenmiş proteinleri, transkripsiyon faktörlerini, mRNA içeren partikülleri, virüsleri, fagozomları, endoplazmik retikulumdan (ER) golgiye geçen vezikülleri, lipid damlacıklarını, lizozomları, melanozomları, peroksizomları, mitokondriyi ve endozomları çekirdeğe doğru taşıdığı bilinmektedir. Nöronlarda, dinein hücre gövdesine retrograd taşınımını yönlendirir ve nöronal göç, büyüme ve sinaps oluşumu için gereklidir. Sitoplazmik dineinlerin fonksiyonunda görülen bozuklukların/aksaklıkların, amyotrofik lateral skleroz, Charcot-Marie-Tooth, Alzheimer, Parkinson ve Huntington gibi birçok nörodejeneratif hastalıklar, lizensefali ve primer silyer diskinezi ile ilişkili olduğu ortaya konulmuştur. Bu belirtilen hastalıklar ile gösterdiği yakın ilişki sebebiyle özellikle tedavi açısından bakıldığında, sitoplazmik dinein motor proteininin nasıl çalıştığına anlaşılması ve çalışırken ne tür fonksiyonel aksaklıkların hastalığa sebep olduğunun belirlenmesi son derece önemlidir. Tıbbi önemlerine ek olarak, dineinler sahip oldukları özgün yapısal organizasyon sebebiyle nanoteknoloji uygulamalar yönünden ve alanında son derece

önemli bir yere sahiptir. Protein mühendisliği uygulanarak yapısında gerçekleştirilecek değişikliklerle dineinler bir bütün olarak veya parçalar halinde nanoteknolojik uygulamalarda kullanılması son yıllarda önemli derecede ilgi çekmeye başlamış bir alan olmuştur.

Dineinler hücre içerisinde iki ağır zincir ve bunlara bağlı küçük peptidlerle dimer halde bulunmaktadır. Dinein ağır zinciri C-terminali motor bölgesi ve N-terminali kuyruk bölgesinden oluşur. Motor bölgesi kafa, sap ve MT bağlanma bölgesinden oluşur. Kafa bölgesi 6 adet AAA+ (AAA1-6)'dan oluşan heksamerik bir halka oluşturur ve bu halkadan 4 adet uzantı çıkmaktadır; kuvvet kolu, sap, payanda ve C-terminal bölgesi. Halka oluşumu AAA ailesinin üyelerinde ortak özelliştir, bu halka oluşumu AAA alt ailesinin protomerleri toplandığında meydana gelir. Miyozinler ve kinesinler ağır zincirlerinde sadece bir ATP bağlanma bölgesine sahipken, dineinlerin baş bölgesindeki AAA bölgelerinin ilk dördü (AAA 1-4) korunmuş Walker A (P-halka (fosfat bağlanma halkası) bölgesi) nedeniyle ATP'yi bağlayabilir ve katalitik aktiviteye sahiptir. AAA1 bölgesi, ATP'nin bağlanmasından ve ATP'nin hareketlilik için güç üretmek üzere hidrolize edilmesinden sorumludur; AAA1 rolünden farklı olarak, AAA3 bölgesi, ATP'nin hidrolize olması nedeniyle AAA1 ve kuvvet kolu arasında yapısal değişiklikler ileten bir düzenleme anahtarı gibi çalışır. Dinein MTBD alanı, kafaya, 10-15 nm uzunluğunda, anti paralel sarmal-sarmal sapla bağlanır.

Dinein mekanokimyasal çevrimi AAA1 bölgesi, kuvvet kolu ve sap arasındaki koordinasyonu gerektirir. Hareketlilikten sorumlu olan AAA1 bölgesinin nükleotit durumu çevrim için önemlidir. Bu nedenle, AAA1 bölgesinin apo, ATP, ADP olarak 3 farklı nükleotit durumuna sahiptir. Dinein sapı, kafa ve dinein MT bağlanma bölgesi arasında iletişimi gerçekleştirmektedir. Bu iletişim, sapın yapısal hareketi ile sağlanır. Sap α ve β olmak üzere iki yapıda bulunabilir; α yapısında dinein MT bağlanma bölgesi yoluyla MT'ye kuvvetli bir şekilde bağlanırken, β yapısında dinein MT'ye bağlı değildir. Dinein kuvvet kolu, dinein mekanokimyasal çevrimi sırasında düz ve bükük yapılar arasında geçiş olacak şekilde konformasyonel değişime uğrar. Kuvvet kolunun düz yapısında pre: güç stroku öncesi, bükük yapısına ise post: güç stroku sonrası yapılar denilmektedir. Kuvvet kolu bükük yapıda iken, N-terminali AAA2-AAA3 ile temas ettiği yerdedir. Kuvvet kolu düz yapıda iken ise N-terminali AAA4'te veya AAA5'te bulunur. Dineinin AAA1 bölgesinde herhangi bir nükleotid bağlı olmadığı durumda kuvvet kolu AAA5'te, ADP bağlı iken ise AAA4'te bulunur.

Dinein motorunun mekanokimyasal çevrimi en az beş farklı termodinamik hal ile (TH1-5) tanımlanabilir. Dinein termodinamik halini tanımlamak için 3 parametre kullanılacaktır. Bunlar AAA1'in nükleotid durumu, sap yapısı ve kuvvet kolunun yapısı olarak sıralanmaktadır. İlk termodinamik halinde (TH1); dinein AAA1 bölgesi Apo durumunda, sap α yapısında ve kuvvet kolu ise düz yapıdadır. (TH1: Apo, α , post). Daha sonra, ATP dineinin AAA1 bölgesine bağlanmakta, dinein MT'den ayrılmakta ve sap α yapısından β yapısına geçmektedir. Bunların sonucunda dinein ikinci termodinamik hale geçmektedir (TH2: ATP, β , post). Ardından, AAA1 bölgesinde ATP hidrolizi başlamaktadır ve kuvvet kolu bükük yapıya geçmektedir. Böylelikle dinein 3. termodinamik hale geçmektedir (TH3: ADP.Pi, β , pre). Daha sonra, dynein MT'ye tekrar bağlanmakta, sap α yapısına geri dönmekte ve AAA1 bölgesinden fosfat salınmaktadır. Bunun sonucunda dinein 4. Termodinamik hale geçmektedir. (TH4: ADP, α , pre). Daha sonra, kuvvet kolu bükük yapıdan düz yapıya doğru hareket edip güç strokunu gerçekleştirmektedir. Bunun sonucunda dinein 5. Termodinamik hale geçmiş bulunmaktadır (TH5: ADP, α , post).

Literatürdeki dinein motor bölgesi yapıları incelendiğinde, sadece TH3 ve TH5 halindeki yapıların bulunduğu görülmüştür. Bu tez çalışmasında, ilk adım olarak kuvvet kolunun TH3 yapısından başlayarak TH2'deki yapısına ulaşma amaçlı olarak bir dizi moleküler dinamik (MD) simülasyonları gerçekleştirilmiştir. Bu amaca yönelik olarak TH5'teki kuvvet kolu yapısı hedef olarak konulmuş ve bu hedefe doğru kuvvet kolu hareketi yönlendirilmiş MD simülasyonları ve kısıtlanmış MD simülasyonlarının bir kombinasyonu olan protokol ile modellenmiştir. Bu modelleme sonucunda ortaya çıkan kuvvet kolu hareketi, sonrasında gerçekleştirilen şemsiye örneklendirilmesi ile detaylandırılmış ve kuvvet kolu hareketi ile ilgili geniş yapısal örnekleme elde edilmiştir.

Çalışmanın başında SMD parametrelerini belirleyebilmek adına literatür çalışması yapılmış ve hız $1 \text{ \AA}/ns$ olarak belirlenmiştir. Daha sonrasında SMD atomlarını ve sabitlenecek atomları belirleyebilmek adına sırasıyla 3 set deneme simülasyonları yapılmış ve kuvvet kolunun modellenmesi için uygun olan parametreler elde edilmiştir. Kuvvet kolunun modellenmesi için yapılan birbirini takip eden 11 MD simülasyonu döngüsü gerçekleştirilmiştir. Her bir MD simülasyonun döngüsünde bir adet SMD simülasyonu ve onu takip eden bir adet kısıtlanmış MD simülasyonu gerçekleştirilmiştir. SMD simülasyonlarında kuvvet kolu üzerinde kuvvet uygulama suretiyle sabit hızda hedefe doğru ilerletilmektedir. Kısıtlanmış MD simülasyonlarında ise kuvvet kolu dış kuvvetlerle SMD sonucunda geldiği pozisyonda sabitlenmektedir. 8. MD döngüsünde kuvvet kolu, dineinin baş yapısı ile yapısal çakışma yaşamıştır. Bu yapısal çakışmanın daha önceden olabileceği literatürde belirtilmiş ancak atomik düzeyde kanıtlanmamıştır. Kuvvet kolunun bükük yapısından başlayarak çakışmanın gerçekleştiği düz yapısına kadar olan geçişin daha detaylı örnekleme için şemsiye örnekleme yapılmıştır. Şemsiye örneklendirilmesinde bir reaksiyon koordinatı belirlenip, sistemin o reaksiyon koordinatının belli bir değerini örnekleme için dış potansiyel uygulanmaktadır. Şemsiye örnekleme için belirlenen reaksiyon koordinatı kuvvet kolunun düz yapısına olan ortalama karesel sapması belirlenmiştir. Şemsiye örnekleme için gerekli olan yapılar MD simülasyon döngülerinin sonlarındaki yapılar seçilmiş ve örneklenebilir yapılar olarak belirlenmiştir. Daha sonrasında elde edilen yapıların dağılımları incelenerek ana bileşenler analizi tüm reaksiyon koordinatı üzerinde gerçekleştirilerek şemsiye örnekleme MD simülasyonları süresince dinein kuvvet kolunun yaptığı başlıca hareketler belirlenmiştir. Daha sonrasında ağırlıklı histogram analizi yöntemi kullanılarak dineinin kuvvet kolunu hareketi sırasında oluşan serbest enerji yüzeyi reaksiyon koordinatının bir fonksiyonu olarak oluşturulmuştur. Elde edilen serbest enerji profiline göre kuvvet kolunun ATP bağlandıktan sonra TH2'den TH3'e geçişi enerjetik açıdan elverişli bir proses olduğu görülmüş olup bunun sonucunda serbest enerji değişiminin $\sim -40 \text{ kJ/mol}$ olduğu görülmüştür. Daha sonrasında ise açığa çıkan enerji farkının nereden geldiğini analiz etmek için kırılan ve yeniden kurulan tuz köprüleri MD simülasyon yörüngeleri boyunca incelenmiş ve reaksiyon koordinatına göre gruplandırılarak, kuvvet kolunun hareketi süresince nerede hangi bağların kurulduğu ve bozulduğu atomik boyutta incelenmiştir. Kuvvet kolu hareketi sırasında 9 tane tuz köprüsünün kırıldığı ve oluştuğu görülmüştür. Bunlardan 6 tanesi düz yapıda, üç tanesi ise bükük yapıda mevcuttur. Kırılan ve tekrardan kurulan tuz köprülerinin serbest enerji yüzeyi ile uyumlu olduğu ve proses için önemli olduğu sonucunda varılmıştır.

Tez çalışması sonucuna, dinein mekanokimyasal çevriminde literatürde henüz tam anlamıyla aydınlatılmamış bir dinein termodinamik hali olan TH2 ile ilgili son derece önemli bilgiler elde edilmiştir.



1. INTRODUCTION

Eukaryotic cells are required intracellular order to perform fundamental activities. Intracellular organization of the eukaryotic cells are provided by cytoskeletal motor proteins that move across the cytosolic tracks, which are microtubules (MT) and actin filaments, by hydrolyzing Adenosine Triphosphate (ATP). These motor proteins take crucial roles in the eukaryotic cells, such as ciliary beating (Gibbons, 1963; Hirokawa, Noda, Tanaka, & Niwa, 2009), muscle contractions (Schliwa, 1999), cell divisions, vesicular transport (Schliwa, 1999), and neuronal development and transportation (Hirokawa et al., 2009).

Cytoskeletal motor proteins are differ in their structure, movement direction, cytosolic tracks that they bind, and the cargos that they carry. These motor proteins are divided in three families, they are kinesin, dynein, and myosin families. Members of kinesin and dynein superfamilies move along the MT, other, myosin family members move along the actin filaments. Kinesin protein family has members that can move to plus (+) or minus (-) end of the MT, similarly myosin motor proteins can also move to barbed (+) or pointed (-) end of the actin filaments (Schliwa, 1999; Wells et al., 1999). Unlike, dynein motor proteins mostly move towards to minus end of the MT (Roberts, Kon, Knight, Sutoh, & Burgess, 2013).

1.1 Myosin

The myosin superfamily is a distinct protein family, members that belong this family are gathered into numerous classes (Odrionitz & Kollmar, 2007). Myosin was firstly found in the muscle cells, and they were found to be responsible for muscle contraction. However, myosins can be found in different cell types and organs (Maupin, Phillips, Adelstein, & Pollard, 1994), and their localization depends to their functional and structural properties (Syamaladevi, Spudich, & Sowdhamini, 2012; Thompson & Langford, 2002). Myosins have generally 1000-2000 amino acids long structure, and constitute from three domains; head domain, which is conserved, has ATPase activity and responsible for movement and actin binding; neck domain

connects head and tail domains, and this domain called light chain with bound regulatory proteins; the tail domain, which is variable, responsible for binding of various cargos, dimerization and oligomerization of myosins (O'halloran, Ravid, & Spudich, 1990; Syamaladevi et al., 2012).

1.2 Kinesin

Kinesin was firstly discovered for their roles in carrying cargos towards to the axon terminal in giant axon of the squid (Brady, 1985; Vale, Reese, & Sheetz, 1985). The kinesin superfamily has 15 members, that most of them move towards to plus-end of the MT, only Kinesin-14 subfamily moves to the minus-end of the MT (Hirokawa et al., 2009; Yamada, Tanaka-Takiguchi, Hayashi, Nishina, & Goshima, 2017), and these members divided into three groups according to the location of the motor domain in the structure: N-Kinesins that move towards to plus end of the MT; C-Kinesins that move towards to minus end of the MT; and M-Kinesins that depolymerize the MT (Dagenbach & Endow, 2004; Hirokawa, 1998). Kinesins have generally 700-1800 amino acids long structure, and, constitute from three domain, like myosins; head domain, which has ATPase activity and is responsible for movement and MT binding; α -helical stalk domain is responsible for dimerization and oligomerization of the kinesins in higher order and connect head and tail domains; tail domain is responsible for binding of various cargos and various subfamily specific functions (Cochran, 2015; Hirokawa et al., 2009).

1.3 Dynein

Dynein was firstly identified in *Tetrahymena pyriformis*' cilia where it responsible for the cilia beating (Gibbons, 1963). Thereafter, two different dynein isoforms were identified; firstly, identified in calf brain where it responsible for movement in the cytoplasm (Cytoplasmic Dynein-1) (Paschal, Shpetner, & Vallee, 1987; Paschal & Vallee, 1987); later, identified in *Chlamydomonas* where it responsible transporting components that needed for flagellar assembly (Cytoplasmic Dynein-2) (Pazour, Dickert, & Witman, 1999; Porter, Bower, Knott, Byrd, & Dentler, 1999). Dyneins are member of AAA+ (ATPases Associated with diverse cellular Activities) family (Neuwald, Aravind, Spouge, & Koonin, 1999), and generally diverged to two main subfamily: axonemal and cytoplasmic dynein (Grotjahn & Lander, 2019; Höök &

Vallee, 2006). Axonemal dynein subfamily is responsible for beating of flagella and cilia; cytoplasmic dynein subfamily is responsible for transporting, directed cell movement, mitosis, and cell polarization (Höök & Vallee, 2006).

Cytoplasmic dynein (referred to hereafter as dynein) interacts with many intracellular pathways. Dyneins carry aggregated proteins (Johnston, Illing, & Kopito, 2002), transcription factors (Harrell et al., 2004), mRNA containing particles (Bullock, Nicol, Gross, & Zicha, 2006), viruses (Dodding & Way, 2011), and membrane-bound organelles, so far known to be transported by dynein: phagosomes (Blocker et al., 1997), vesicles that move from the endoplasmic reticulum (ER) to golgi (Presley et al., 1997), lipid droplets (Gross, Welte, Block, & Wieschaus, 2000), lysosomes (Jordens et al., 2001), melanosomes (Gross et al., 2002), peroxisomes (Kural et al., 2005), mitochondria (Pilling, Horiuchi, Lively, & Saxton, 2006), and endosomes (Driskell, Mironov, Allan, & Woodman, 2007), towards the nucleus. In neurons, dynein drives retrograde transport towards the cell body (Schnapp & Reese, 1989) and is required for neuronal migration (Sasaki et al., 2000), growth (Barakat-Walter & Riederer, 1996), and synapse formation (Cheng et al., 2006). Numerous neurodegenerative diseases, such as degeneration (Hafezparast et al., 2003) and sensory neuropathy in motor neurons (El-Kadi, Soura, & Hafezparast, 2007), amyotrophic lateral sclerosis (ALS) (Soo, Farg, & Atkin, 2011), Alzheimer's disease, Huntington's disease, Parkinson's disease, lissencephaly, and schizophrenia (Eschbach & Dupuis, 2011), are related with the glitch in dynein motility. Dynein also plays important roles in cell division, such as maintenance of the proper tension and length of the spindle (Gaetz & Kapoor, 2004), focusing MTs into spindle poles (Heald et al., 1996), and regulation of the spindle assembly checkpoint activation and proper chromosome segregation (Howell et al., 2001).

1.3.1 Dynein structure

Dynein is present in dimer form (1.4 MDa) in the cell, and constitutes two identical dynein heavy chains (DHCs) and associated small peptides (Perrone et al., 2003). While myosins' and kinesins' heavy chain size in broad range, DHCs have similar size, which is between 471 and 540 kDa (Holzbaur & Vallee, 1994; Vallee & Sheetz, 1996). DHC is composed of a C-terminal motor domain and an N-terminal tail domain. The head constitutes a hexameric ring of six AAA+ (AAA1-6, 15 nm in diameter) and four extensions emerge from the hexameric ring of dynein; the linker, the stalk, the

buttress, and the C-terminal domain (Burgess, Walker, Sakakibara, Knight, & Oiwa, 2003). Ring formation is common property in members of AAA superfamily, this ring formation occurs when protomers of AAA subfamily are collocated (Vale, 2000). Dyneins also form hexameric ring, nevertheless, all AAA modules are sorted into one single polypeptide (Vale, 2000). While myosins and kinesins have only one ATP binding site at their heavy chain, dyneins' first four of the AAA modules (AAA1-4) of the head can bind ATP due to conserved Walker A (P-loop (phosphate binding loop) domain) motifs and have catalytic activity (Ogawa, 1991). AAA1 module is responsible for binding ATP and hydrolyzing ATP to generate power for motility (Bhabha et al., 2014); unlike AAA1 role, AAA3 module works like a regulatory switch, that transmits conformational changes between AAA1 and linker, due to hydrolyzing ATP (Kon, Nishiura, Ohkura, Toyoshima, & Sutoh, 2004). MTBD domain of dynein is connected to head with stalk, which can be 10-15 nm long, antiparallel coiled-coil.

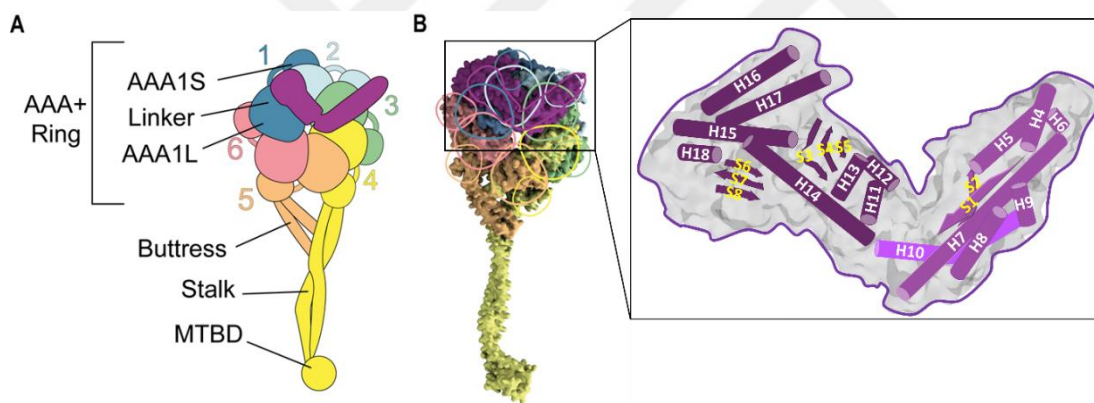


Figure 1.1 : Schematic representation of Dynein and Linker. A) Illustrative representation of cytoplasmic dynein domains linker, AAA+ ring, buttress, stalk and MTBD. B) Crystal structure of the cytoplasmic dynein (PDB ID 4RH7 (Schmidt, Zalyte, Urnavicius, & Carter, 2015)) shown in surface representation using the same color selection as in A). On the right hand side, the static region of the linker (H11-H18) is shown in a darker tone of magenta while the rigid-body moving region of the linker (H5-H9) is shown in a lighter tone. Hinge helix (H10) is shown in violet.

1.3.2 Dynein mechanochemical cycle

The cytoskeletal motors have differences in many aspects, but they follow similar mechanochemical cycle which is done by successive steps that ended with movement of the associated cargos. Dynein mechanochemical cycle relatively complex the other motor proteins. Because of the dynein mechanochemical cycle requires the coordination between the AAA1 module, the stalk, and the linker. AAA1 module

responsible for the motility, so, nucleotide state of the AAA1 module is important for the cycle. Therefore, AAA1 module has 4 different nucleotide states apo, ATP, ADP.Pi, ADP. Stalk of the dynein requires for the communication of the head and MTBD of dynein. This communication is provided by movement of the stalk registry. There is two stalk registry α and β ; while, in α registry dynein strongly bounded to the MT via MTBD, in β registry dynein released from the MT. The last part of the coordination is linker. Linker is important for the movement of the dynein, it connects the dynein head and tail domain. Dynein linker undergoes the conformational change during the mechanochemical cycle, and has two different states; pre: pre-powerstroke state that the linker is in a bent conformation and where its N-terminus contacts AAA2-AAA3 (Gee, Heuser, & Vallee, 1997; Kon et al., 2004), and post: post-powerstroke state, the linker is in a straight conformation, when the AAA1 domain of the dynein is empty or ADP bound, the linker is in a straight conformation and exiting the ring at AAA4 (Kon et al., 2004; Schmidt et al., 2015). The mechanochemical cycle of the dynein motor can be described at least five distinct thermodynamic states (TS1-5). States will indicated by four indicators; (Thermodynamic State Number: nucleotide state of AAA1, stalk registry, and linker conformation). At the first thermodynamic state (TS1); AAA1 module of the dynein in the Apo state, stalk registry in α state, and the linker straight conformation (TS1: Apo, α , post). Subsequently ATP binding to the AAA1 module triggers MT release (Burgess et al., 2003) of the dynein due to shift occurs in the stalk from the α registry to the β registry (TS2: ATP, β , post) (Kon et al., 2009; Kon et al., 2004). Then, ATP hydrolysis starts in the AAA1 domain, and the linker into the bent conformation (TS3: ADP.Pi, β , pre). Dynein stepping towards to the minus-end due to generated net bias by the conformational change, which called as the priming stroke (Kon et al., 2012; Roberts et al., 2009; Schmidt, Gleave, & Carter, 2012). After, dynein rebinds the MT, stalk coiled-coils shift back to the α registry, and the phosphate released from the AAA1 module (TS4: ADP, α , pre). Subsequently, the linker moves from the bent to the straight conformation. This is referred to as force-generating powerstroke (TS5: ADP, α , post) (Kon et al., 2012; Roberts et al., 2009; Schmidt et al., 2012). Dynein is expected to switch back to state 1 after ADP release without significant conformational arrangement of its stalk and the linker.

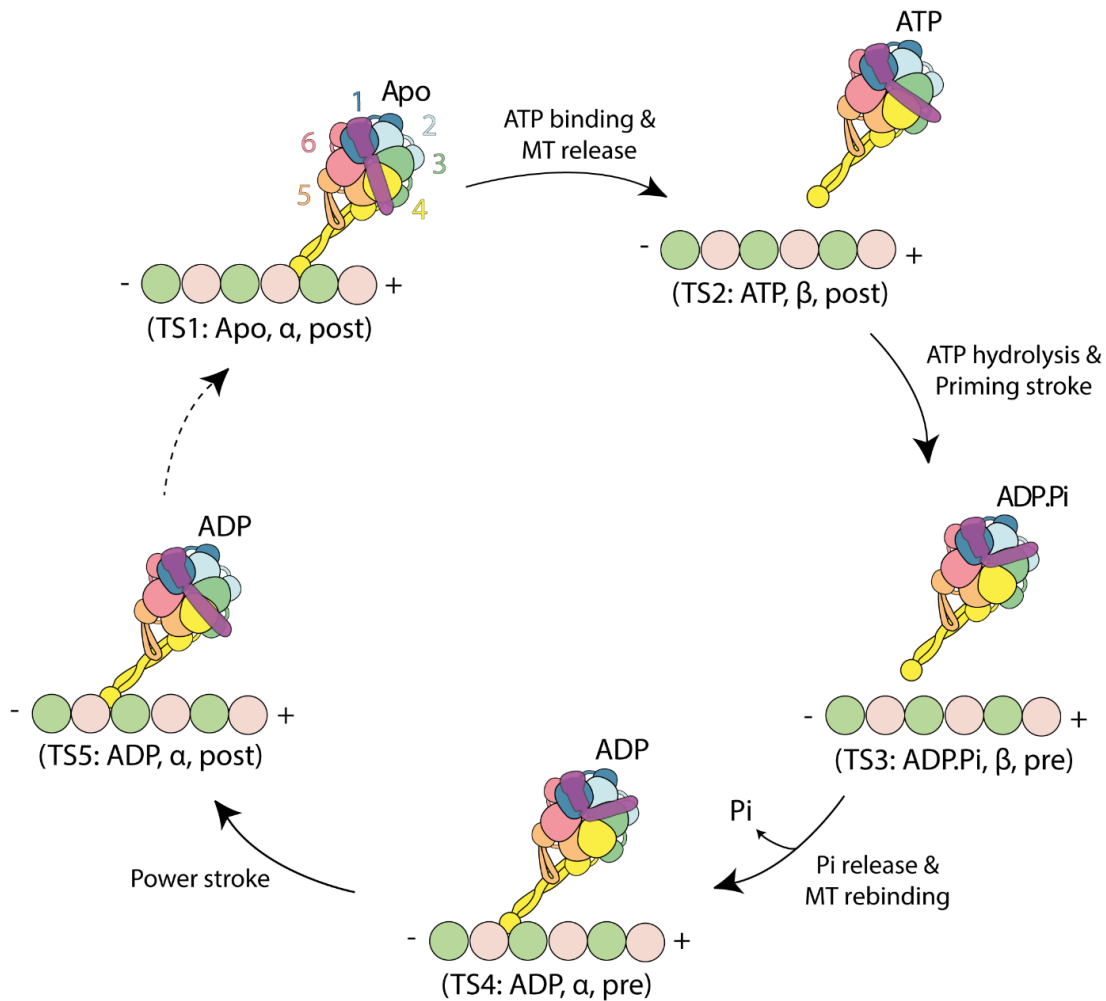


Figure 1.2 : Mechanochemical cycle of the dynein. The AAA+ ring is composed of six AAA domains and binds to MTs through a coiled-coil stalk with a small MTBD. The linker undergoes ATP dependent conformational changes and generates force and motility, synchronized with MT binding/unbinding cycles.

1.3.3 Linker

The linker is composed by four domains: Link1-4. Link1 domain including H4-H7 helices, Link2 domain including H7-H9 helices, Link3 domain including H11-H14 helices, and Link4 domain including H15-H18 helices (Kon et al., 2012; Schmidt et al., 2012). The region Link3-4 stays rigid during the linker transformation and does not move with respect to the AAA ring (Fig. 3 A). The region Link1-2 performs rigid body motion, where it is in contact with AAA4-5 in its (TS5: ADP, α , post) straight form and in contact with AAA2-3 in its (TS1: Apo, α , post) bent form. H10 acts as a hinge and adopts a curved/bent conformation upon linker movement. Schmidt et al. (Schmidt et al., 2015) superimposed the straight linker structure of dynein (TS5: ADP, α , post) onto the bent linker structure of dynein (TS3: ADP.Pi, β , pre) via Link3-4. This alignment resulted in an overlap between Link1-2 of the straight linker structure

and AAA4 of dynein (TS3: ADP.Pi, β , pre). Based on the available crystal structures, their conclusion was that ADP.Vi binding to AAA1 site induces linker bending through the closure of AAA1/AAA2 ring. This, in turn, induces a steric clash between the linker and AAA4, driving it into a bent conformation that is primed to produce force.





2. METHODOLOGY

2.1 MD Simulation Details

Initial conformation of this study was selected from the dynein (TS3*: ATP, β , pre) motor domain MD simulations in our previous study (Can, Lacey, Gur, Carter, & Yildiz, 2019). In the previous study, pre-power stroke conformation of the human dynein-2 (PDB 4RH7 (Schmidt et al., 2015)) structure had been used, mutated residues were reversed and missing residues were completed. Obtained structure was solvated in a water box using TIP3P explicit water model having at least 15 Å cushion of water in each direction by using “Solvate Plugin” of VMD (Humphrey, Dalke, & Schulten, 1996). Solvated system was ionized with 1 mM MgCl₂ and 150mM KCl, then ionic charge of the total system was neutralized with KCl. At the end, obtained system constitutes of 781,332 atoms. 3 sets of MD simulations were performed for dynein (TS3*: ATP, β , pre) and the final conformation of the first set was selected for our current study. Please refer to our earlier study (Can et al., 2019) for MD simulations details.

In this study, all simulations were performed in NAMD 2.13 (J. C. Phillips et al., 2005) (with both NVIDIA CUDA acceleration and multicore versions) using the CHARMM36 all-atom additive protein force field (Best et al., 2012). Time step of the simulations were set to 2 fs. van der Waals (vdW) interactions were truncated at 12 Å cut-off distance. Long-range electrostatic forces were calculated using Particle-Mesh Ewald (PME) method. The simulations were performed under *NPT* conditions, constant particle (*N*), constant pressure (*P*), and constant temperature (*T*), temperature were kept at 310 K, and pressure were kept at 1 atm. Langevin dynamics were used for maintaining isothermal conditions with 1 ps⁻¹ of damping coefficient. For maintaining pressure constant, 100 fs of the oscillation period and 50 fs of damping time scale were used in Langevin Nosé-Hoover method. Simulations were recorded every 5 ps.

2.2 Modelling the Linker Movement of Dynein with Steered MD Simulations

2.2.1 Theory

The major dynein movements takes place in during the following transitions of the dynein mechanochemical cycle: (TS2: ATP, β , post) \rightarrow (TS3: ADP.Pi, β , pre), and (TS4: ADP, α , pre) \rightarrow (TS5: ADP, α , post). However, only two complete structures of dynein motor (TS3 (4RH7) and TS5 (3VKG)) are available in the literature. Furthermore, general assumption for the linker structure in the literature, linker structure of TS1, TS2, and TS5 can be accepted as similar. So, linker structure of TS2 was taken from linker structure of TS5, as a representatively. We have procured full length dynein motor in (TS3*: ATP, β , pre) form well equilibrated, and it is used as initial structure for MD simulations. For modeling the linker transition from (TS2: ATP, β , post) to (TS3: ADP.Pi, β , pre), this transition was modeled in reverse direction of the mechanochemical cycle by application of external work: from (TS3*: ATP, β , pre) to (TS2: ATP, β , post). The required work is applied to the system via SMD and TMD simulations and the movement of the linker is performed.

Probing biological processes on time scales that accessible to MD simulations are done with Steered MD (SMD) simulations, and can be used for defining the binding pathway of ligands and explaining the elastic properties of proteins (Isralewitz, Gao, & Schulten, 2001). Applying external force to the atom or atoms along a vector to pull is form the core idea of SMD simulations. The pulling process can be carried out at a constant speed or by applying a constant force (J. Phillips, Isgro, Sotomayor, & Villa, 2003).

In this study, constant velocity pulling was performed. The center of mass of a group of ‘steered’ atoms (referred to hereafter as SMD atoms) binds to a dummy atom with a virtual spring. The dummy atom is pulled at a constant velocity along the ‘pulling direction’ and the following force is applied along the vector to the SMD atoms,(J. Phillips et al., 2003)

$$\mathbf{F} = -\nabla U \quad (1)$$

$$U = \frac{1}{2}k[\mathbf{v}t - (\mathbf{R} - \mathbf{R}_0) \cdot \mathbf{n}]^2 \quad (2)$$

Here, the potential energy refers as U , the spring constant refers as k , the pulling velocity refers as \mathbf{v} , the time refers as t , the current coordinates of the center of mass

of the SMD atoms refer as \mathbf{R} , the initial coordinates of the center of mass of SMD atoms refer as \mathbf{R}_0 , and the direction of pulling refers as \mathbf{n} (J. Phillips et al., 2003).

While Linker1-2 (E1257-G1396, in human dynein-2) domain performs a rigid body motion, Linker 3-4 (P1427-Q1650, in human dynein-2) domain stays static during the linker swing motion. When the dynein linker structure comparison of between (TS3: ADP.Pi, β , pre) and (TS2: ATP, β , post) states were showed that; static region has an RMSD of 1.79 Å, when alignment through C^α atoms of this region, and linker region that performs rigid body motion has an RMSD of 1 Å, when alignment through C^α atoms of this region. H10 comprising residues I1397-A1425 residues acts as hinge. Static regions of dynein (TS3*: ATP, β , pre) and (TS2: ATP, β , post) linker were aligned for defining SMD pulling vector. Subsequently, the vector pointing from the center of mass coordinates of SMD atoms in (TS3*: ATP, β , pre) to those in (TS2: ATP, β , post) was constructed (Fig. x A).

2.2.2 Selection of SMD simulation parameters

According to the SMD simulation theory, selection of the spring constant should be determined by the SMD atoms can closely follow the reaction coordinate (satisfying stiff-spring approximation), but yet soft enough to allow small deviations (Israelewitz et al., 2001). This means that, the thermal oscillations of the linker are in the order of applied external forces, therefore, the process proceeds close the equilibrium during the SMD simulations.

A three set of SMD atoms and fixed atoms selection were tested to determine the best selection of atoms yielding minimal internal structural deformation in the static and rigid-body moving regions of the linker, while successfully steering the linker towards its target structure. In this study, the pulling velocity of 1 Å/ns was selected. And, spring constants of 10, 25, 50, 75, and 100 kcal/mol/Å² were tested for determining optimal spring constant for SMD simulation.

At the first trial, L1264, L1309, and V1325 residues, which found on almost the tip of the linker1-2 domain helices, were selected as SMD atoms, and L1415 and N1416 residues were selected as fixed atoms. Pulling direction was selected from the center of mass of the C^α atoms of the residues L1264, L1309, and V1325 to the center of mass of the C^α atoms of corresponding residues on *Dictyostelium discoideum* dynein, which are L1531, I1572, and A1588. First trial was immediately failed, structural

deformations were observed on the linker structure. After that, fixed atoms were expanded to residues L1415-A1425. For this trial, first simulations were performed successfully and $25 \text{ kcal/mol}/\text{\AA}^2$ was selected for further simulations as it was large enough. But, structural deformations were observed in the further simulations. Then, SMD atoms and fixed residues were changed and expanded. C^α atoms of residues G1256-G1271 (H4), K1296-K1313 (H5), and E1322-W1349 (H7) were selected as SMD atoms. Based on the sequence alignment (Fig. 3 B) the corresponding residues on *Dictyostelium discoideum* dynein, which will be selected as the end point of the pulling direction vector, are G1523-W1538 (H4), D1559-K1576 (H5), and E1585-W1612 (H7). During the steering process, C^α atoms of L1415-A1424 (H10-hinge) and D1434-G1442 (H12) were kept fixed. After, spring test simulations, $50 \text{ kcal/mol}/\text{\AA}^2$ was selected for further simulations.

Dynein linker was pulled for 5 ns, which means dummy atom was moved by 5 \AA along the pulling direction. Subsequently, 5 ns of constrained MD (CMD) simulations were performed. The aim of performing the CMD simulations are correcting the structural deformation that occurred in the SMD simulations in H4-H10. Furthermore, CMD simulations allow the dynein motor structure to optimize around this new conformation of the linker. Since H4-H9 perform rigid body transition during linker movement, constrains center for H4, H5 and H7 C^α atoms were set by aligning H4, H5 and H7 of dynein (TS3*: ATP, β , pre) to the end conformer of SMD. In addition, constrains were also applied to residues G1256-G1271 (H4), K1296-K1313 (H5), E1322-W1349 (H7), L1415 - A1424 (H10) and D1434 - G1442 (H12). Force constants of $1 \text{ kcal/mol}/\text{\AA}^2$ were applied for the harmonic constrains.

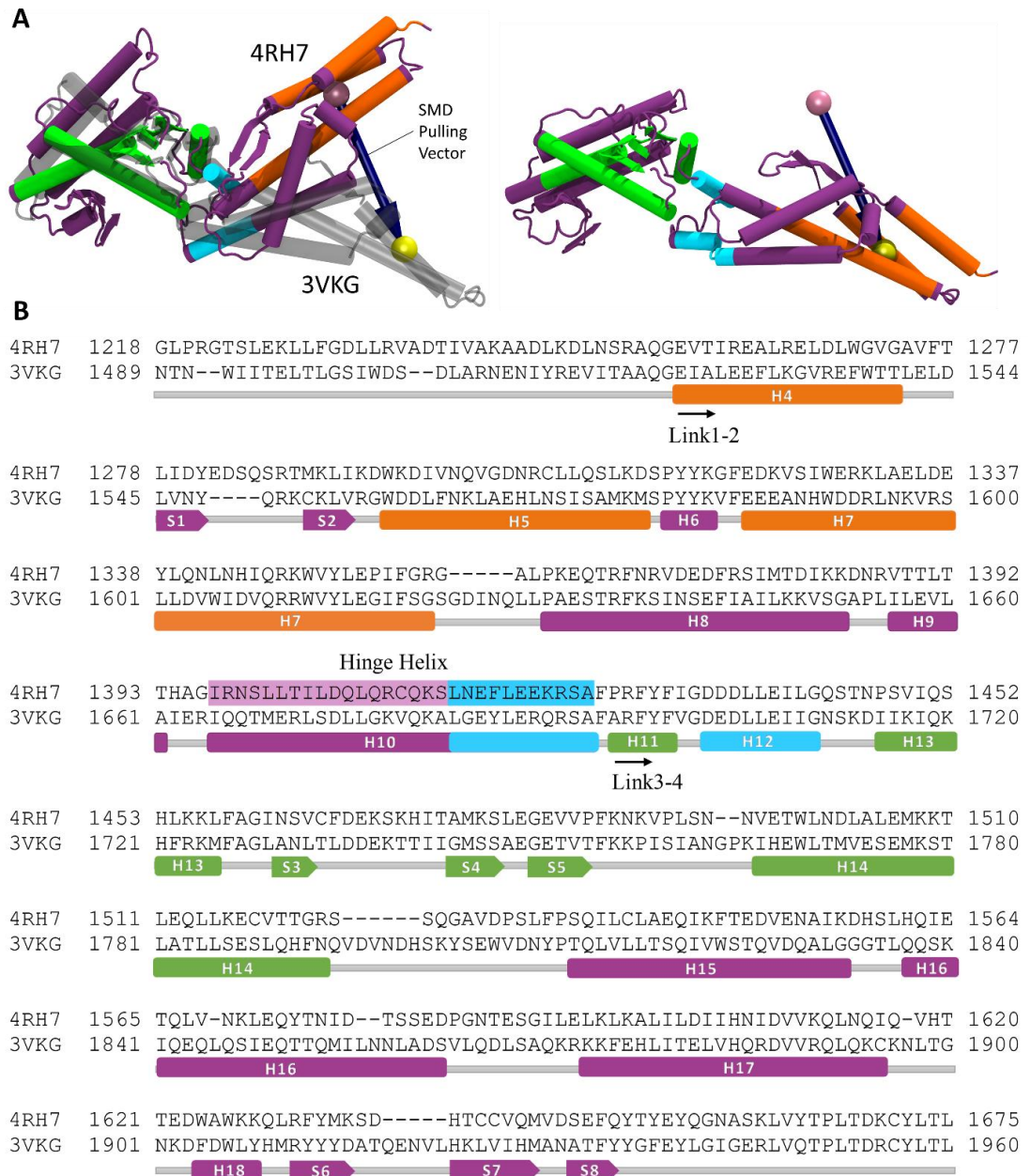


Figure 2.1 : Alignment of the cytoplasmic dynein linker in bent conformation (PDB: 4RH7) with straight conformation (PDB: 3VKG). A) Linker bent conformation (Purple) and straight conformation (transparent grey). Orange color indicated residues are SMD atoms, green color indicated residues are aligned atoms, and cyan colored atoms are fixed atoms. B) Sequence alignment is performed for two structures and sequences of the alpha helices and beta sheets are shown in the alignment.

2.3 Modelling the Linker Movement with Targeted MD Simulations

2.3.1 Theory

In TMD simulations (Engels, Jacoby, Krüger, Schlitter, & Wollmer, 1992; Schlitter, Engels, & Krüger, 1994) a bias potential in addition to the usual MD force field is applied to accomplish (usually large) conformational changes, which are otherwise not accessible at standard MD simulations lengths. For TMD simulations performed using the NAMD software package, the selected subset of atoms in the simulation is guided towards a final 'target' structure by means of steering forces which are evaluated as the gradient of the following potential

$$U_{TMD} = \frac{1}{2} \frac{k}{N} [RMSD(t) - RMSD^*(t)]^2 \quad (3)$$

Here, $RMSD(t)$ is the instantaneous best-fit root mean square deviation (RMSD) of the current coordinates from the target coordinates. The term $RMSD^*(t)$ evolves linearly from the initial RMSD at the first TMD step to the final RMSD at the last TMD simulation step. k is the spring constant and N is the number of selected subset of atoms to be biased toward the target (targeted atoms).

We have selected the C^α atoms of residue stretches G1256-G1271 (H4), K1296-K1313 (H5), E1322-W1349 (H6), L1415-S1424 (H10), D1434-G1442 (H12), P1447-L1457 (H13), I1461-F1466 (S3), H1472-S1478 (S4), V1483-P1491 (S5), V1496-V1523 (H14), S1536-D1550 (H15) of the dynein linker as the subset of atoms to be guided via TMD simulations. Linker structure of 3VKG was selected as the TMD target structure. Spring constants 50, 100, 200, and 400 $kcal/mol/\text{\AA}^2$ were tested, among which $k=400 kcal/mol/\text{\AA}^2$ was strong enough for $RMSD(t)$ to follow $RMSD^*(t)$ closely.

2.4 Umbrella Sampling and Weighted Histogram Method for Free-Energy Calculations

In conventional MD simulations, sampling of the microscopic system of interest with rare conformations almost impossible within the available computing time. Because, the system can be samples the global minimum. At this position, system could not climb over the energy barriers for a long time. For overcome this obstacle, Torrie and Valleau developed a sampling method that called Umbrella Sampling (US) (Torrie &

Valleau, 1977). In this method, the system is simulated with an artificial biasing potential, this also called window potential, to sample the neighborhood of chosen ξ . For probing whole sampling space of the system, multiple US simulations are required. In Umbrella Sampling, MD simulations are performed using a modified potential energy function of the following form (Kumar, Rosenberg, Bouzida, Swendsen, & Kollman, 1992; Souaille & Roux, 2001)

$$U_i(\mathbf{R}) = U_o(\mathbf{R}) + H_i(\xi(\mathbf{R})) \quad (4)$$

Here, the $3N$ -dimensioned vector defines protein structure (N is the total atom number) refers as \mathbf{R} . The potential energy of the molecular system refers as $U_o(\mathbf{R})$, the reaction coordinate (or coordinate of interest) refers as ξ , and some perturbing potential refers as $H_i(\xi(\mathbf{R}))$. By adjusting $H_i(\xi(\mathbf{R}))$ any region along the reaction coordinate can be sampled.

In the present study, ξ is the RMSD of the linker conformation with respect to its target structure (PDB ID: 3VKG). $H_i(\xi(\mathbf{R}))$ is selected to be an harmonic restraint to the reaction coordinate having ξ_i as equilibrium position and k_i as force constant. Thus, the modified energy function is written as,

$$U_i(\mathbf{R}) = U_o(\mathbf{R}) + \frac{1}{2}k_i(\xi(\mathbf{R}) - \xi_i)^2 \quad (5)$$

A force constant of $k_i = 25 \text{ kcal/mol}/\text{\AA}^2$ except two UMD simulations, for these simulations $k_i = 50 \text{ kcal/mol}/\text{\AA}^2$ were used in all UMD simulations. Upon performing MD simulations with modified potential energy functions a set of biased probability distributions $P_i^{(b)}(\xi)$ can be obtained as,

$$P_i^{(b)}(\xi) = \exp[-\beta\Phi_i(\xi)] = \langle \delta[\xi(\mathbf{R}) - \xi_i] \rangle \quad (6)$$

$\Phi_i(\xi)$ is the PMF associated with ξ if the simulation is carried out with the perturbing potential $H_i(\xi(\mathbf{R}))$. From MD trajectories $P_i^{(b)}(\xi)$ can be computed as the normalized histogram of the values occurring during simulation i . The corresponding unbiased probability distribution is defined as,

$$P_i^{(u)}(\xi) = \exp[\beta(H_i(\xi) - f_i)]P_i^{(b)}(\xi) \quad (7)$$

f_i is the free energy coming from the adding of the biasing potential $H_i(\xi(\mathbf{R}))$ to $U_o(\mathbf{R})$. The Weighted Histogram Analysis Method (WHAM) (Kumar et al., 1992) is

an efficient method to recombine the unbiased histograms $P_i^{(u)}(\xi)$ obtained from umbrella sampling simulations to get the total probability distribution $P_o(\xi)$. Once $P_o(\xi)$ is computed, the PMF can be evaluated by $\Phi_i(\xi) = -\frac{1}{\beta} \ln[P_o(\xi)]$. The main steps of WHAM be listed as follows the total probability distribution in WHAM is expressed as follows,

$$P_o(\xi) = C \sum_{i=1}^N P_i(\xi) P_i^{(u)}(\xi) \quad (8)$$

Here total probability distribution $P_o(\xi)$ is written as a linear ξ -dependent combination of $P_i^{(u)}(\xi)$, N is the total number of MD simulations, and n_i is the number of coordinate sets in the i^{th} MD simulation to compute $P_i^{(b)}(\xi)$, $P_o(\xi)$ is total probability distribution, and C is a normalization constant, C calculated by,

$$C = \frac{1}{\beta} \ln D \quad (9)$$

$$D = \frac{Z_0}{Z_i} \quad (10)$$

where the Z is the partition function of the system and D is also constant. For the normalization of weights followed equation is used,

$$\sum_{i=1}^N P_i(\xi) = 1 \quad (11)$$

for each ξ value, the statistical error of the total probability distribution minimized,

$$\frac{\partial(\sigma^2[P_o(\xi)])}{\partial P_i} = 0 \quad (12)$$

then $P_o(\xi)$ obtained as,

$$P_o(\xi) = C \sum_{i=1}^N \frac{n_i}{\sum_{j=1}^N n_j \exp[-\beta(H_j(\xi) - f_j)]} P_i^{(b)}(\xi) \quad (13)$$

All terms in Eq.5 are not readily available (can directly computed) except the free energy parameters $\{f_i\}$. To evaluate $\{f_i\}$ the following equation is solved iteratively,

$$\exp[-\beta f_i] = C \int d\xi \sum_{i=1}^N \frac{n_i \exp[-\beta H_k(\xi)]}{\sum_{j=1}^N n_j \exp[-\beta(H_j(\xi) - f_j)]} P_i^{(b)}(\xi) \quad (14)$$

Iterations start with a guessed value $\{f_i^0\}$. f_i^0 values are used to compute the right hand side of Eq. 9 and by doing so a new set of parameters $\{f_i^1\}$ is evaluated. This procedure is repeated for l steps until convergence in $\{f_i^l\}$ values are observed. The relative error of the WHAM can be computed by,

$$\frac{\delta\Omega(\xi)}{\Omega(\xi)} = \left[g^{-1} \sum_{i=1}^R N_i(\xi) \right]^{-1/2} \quad (15)$$

Here is the g overall factor with $g = 1 + 2\tau$ and g values can be omitted. In addition to that, error estimation of the PMF calculation was computed by integrated method to the Gorsfield's implemented code, which is Bootstrapping technique. In this estimation, normalization cumulant factor $c(\xi)$ is computed and random numbers are generated between 0 and 1, R , and $c(\xi) = R$ computed for ξ . WHAM calculations were performed in MATLAB (The MathWorks, 2019) via the MDToolbox (Matsunaga, 2015).

2.5 Covariance Matrix and Principle Component Analysis

Linker conformations sampled during MD simulations were aligned with the bent crystal structure using the C^α atoms. Using the aligned linker coordinates, the covariance matrix is generated as follows,

$$\mathbf{C} = \langle (\mathbf{R} - \langle \mathbf{R} \rangle) (\mathbf{R} - \langle \mathbf{R} \rangle)^T \rangle \quad (16)$$

Here, \mathbf{R} is the $3 \times 400 = 1200$ dimensional configurational vector composed of the instantaneous C^α atom coordinates of the linker. $\langle \mathbf{R} \rangle$ is the trajectory average of \mathbf{R} . Eigenvalue decomposition of \mathbf{C} is performed and principal components (PCs) are obtained as follows,

$$\mathbf{C} = \sum_{i=1}^{3N} \sigma_i \mathbf{p}_i \mathbf{p}_i^T \quad (17)$$

Here, \mathbf{p}_i is the i^{th} PC and σ_i is the constant is the corresponding variance. Thus, σ_i scales with the magnitude of motion along \mathbf{p}_i . PCs are ordered in descending order

with respect to their σ_i values. Since PC1 and PC2 have the largest two variances, making \mathbf{p}_1 and \mathbf{p}_2 are the most dominant motions observed in the MD simulations. Projections of instantaneous coordinates along PCs are evaluated as $\mathbf{r}_i = \mathbf{p}_i^T (\mathbf{R} - \langle \mathbf{R} \rangle)$.



3. RESULTS & DISCUSSION

3.1 Selection of SMD Parameters

The linker swing movement during the priming stroke was modelled using recursively cycles of SMD and CMD simulations for each 5 ns long, respectively. These simulations were followed (TS3*: ATP, β , pre) \rightarrow (TS2: ATP, β , post) linker transition pathway. The linker was aimed to pull through 5 Å, along the pulling direction. To determine the SMD parameters, 3 different set of simulations were performed. At first trial, the center of mass of the C $^{\alpha}$ atoms of the residues L1264, L1309, and V1325 was selected as SMD atoms, and the C $^{\alpha}$ atoms of L1415 and N1416 residues were selected as fixed atoms. After the 5 ns of SMD simulations, structural deformations were observed for each spring constants. The second set of trial simulations were performed with extended fixed atoms, which residues were the C $^{\alpha}$ atoms of L1415-A1425. After 5 ns of SMD simulations, structural deformations were not observed. And, displacement of the SMD atoms and Dummy atom displacement were plotted for determining optimum spring constant for the SMD simulations, are shown in Figure 3.1.

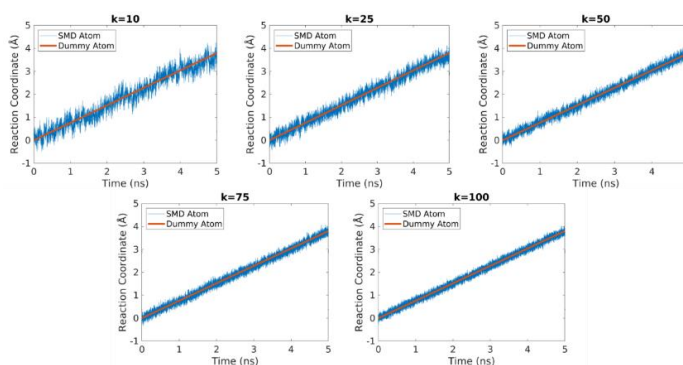


Figure 3.1 : Spring constant selection for the SMD simulations. Second trial of SMD simulations for the pulling velocity of 1 Å/ns was selected. And, spring constants of 10, 25, 50, 75, and 100 kcal/mol/Å² parameters; SMD atoms were the C $^{\alpha}$ atoms of the L1264, L1309, and V1325 residues, and fixed atoms were the C $^{\alpha}$ atoms of L1415-A1425 residues. Blue lines indicates displacement of the SMD atoms and red line indicates the displacement of dummy atom.

As can be seen in figure, SMD atoms fluctuated more for the $10 \text{ kcal/mol/\text{Å}^2}$ spring constant, and SMD atoms followed the dummy atom closely for 50, 75, and 100 $\text{kcal/mol/\text{Å}^2}$ spring constants. These spring constants did not let the SMD atoms fluctuation. So, $25 \text{ kcal/mol/\text{Å}^2}$ spring constant was chosen for further simulations. But, structural deformations were observed at the end of the fifth cycle is can be seen in Figure 3.2.

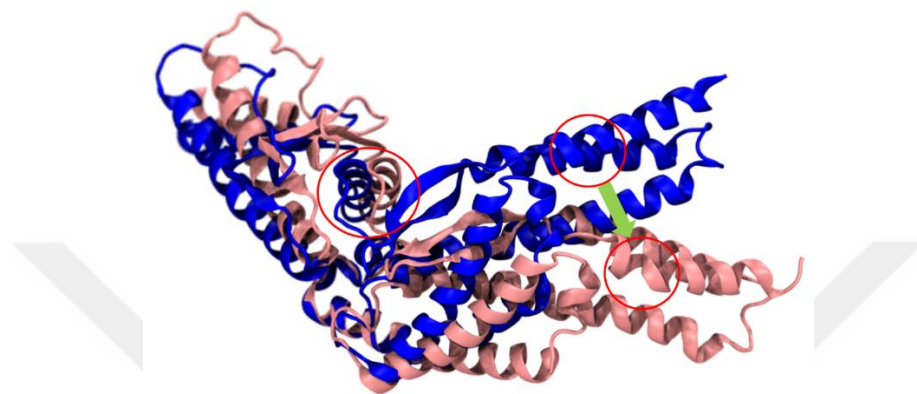


Figure 3.2 : Structural deformations. Initial structure of the linker shown in blue and structure obtained from 5th SMD simulation shown in pink. In the red circle shown on the left, a structural shift was observed in the hinge region compared to the initial structure. In the red circle shown on the right, structural disruptions in the alpha helices of linker is observed, while it is expected to be rigid.

At the third trial, both SMD and fixed atoms were extended; the C^α atoms of residues G1256-G1271 (H4), K1296-K1313 (H5), and E1322-W1349 (H7) were selected as SMD atoms and, C^α atoms of L1415-A1424 (H10-hinge) and D1434-G1442 (H12) were selected as fixed atoms. Same selections simulations were performed for this set, are shown in Figure 3.3.

As can be seen in figure, SMD atoms fluctuated more for the $10 \text{ kcal/mol/\text{Å}^2}$ spring constant, for the $25 \text{ kcal/mol/\text{Å}^2}$ spring constant, SMD atoms followed the dummy atom from slightly behind after 3.5 ns, and SMD atoms followed the dummy atom closely for 75, and 100 $\text{kcal/mol/\text{Å}^2}$ spring constants. These spring constants did not let the SMD atoms fluctuation. So, $50 \text{ kcal/mol/\text{Å}^2}$ spring constant was chosen for further simulations.

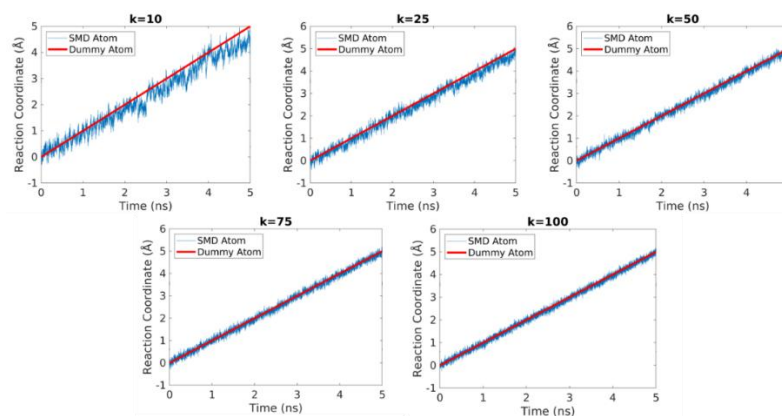


Figure 3.3 : Spring constant selection for the SMD simulations. Second trial of SMD simulations for the pulling velocity of 1 \AA/ns was selected. And, spring constants of 10, 25, 50, 75, and 100 kcal/mol/\AA^2 parameters; SMD atoms were the C^α atoms of G1256-G1271 (H4), K1296-K1313 (H5), and E1322-W1349 (H7) residues, and fixed atoms were the C^α atoms of L1415-A1424 (H10-hinge) and D1434-G1442 (H12) residues. Blue lines indicates displacement of the SMD atoms and red line indicates the displacement of dummy atom.

3.2 Modelling the Linker Priming Stroke Reveals Steric Clash Between the Linker and AAA4

For each SMD simulation followed by subsequent CMD simulations. CMD simulations were aimed to optimize the dynein structure in the new linker conformation. This cycle was proceeded for 11 times: total 110 ns in length. During this cycle, SMD pulling direction was updated before each SMD simulation beginning. The displacement of SMD atoms along the pulling directions for the complete set of SMD-CMD simulations is shown in Figure 3.4A. The evolution of RMSD between the generated/sampled linker conformations and the extended linker structure during these simulations is depicted in Figure 3.4B.

As can be seen in Figure 3.4, after 80 ns of MD simulations (i.e. the 8th cycle), SMD simulations were not able to further move along the pulling direction and decrease its RMSD to the straight linker structure. The reason of this obstacle was the steric clash due to the contact between the linker and the AAA4, shown in Figure 3.5. In the MD simulations, the observed steric clash took place due to the contact of linker residues in H5 (R1306, Q1310, K1313, D1314), the loop between H5-H6 (S1315), H6 (P1316, Y1318, K1319), H7 (E1322, DP1323, V1325, S1326, E1329, R1330, A1333, E1337), and H10 (R1398) with residues in AAA4L PS-I insert (E2742, E2745, P2746, L2748, L2749, P2750, K2752, D2753, S2756, F2761, G2762, P2763, V2764, F2765).

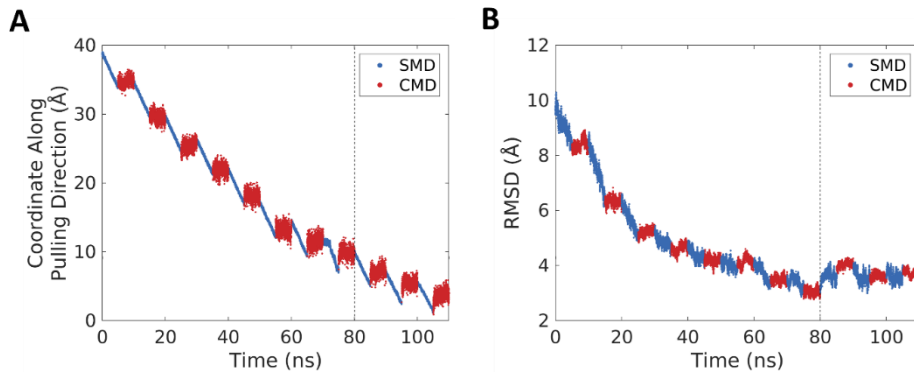


Figure 3.4 : Progress of SMD simulation protocol towards the target linker structure. A) Movement of the center of mass of the pulled atom along the trajectories of SMD and CMD simulations. Blue lines represent the SMD simulations and red lines represent the CMD simulations. B) Change in the RMSD according to the target linker structure in TS1 (3VKG). Blue lines represent the SMD simulations and red lines represent the CMD simulations. The line on the 80. ns points out that the values after there won't be used.

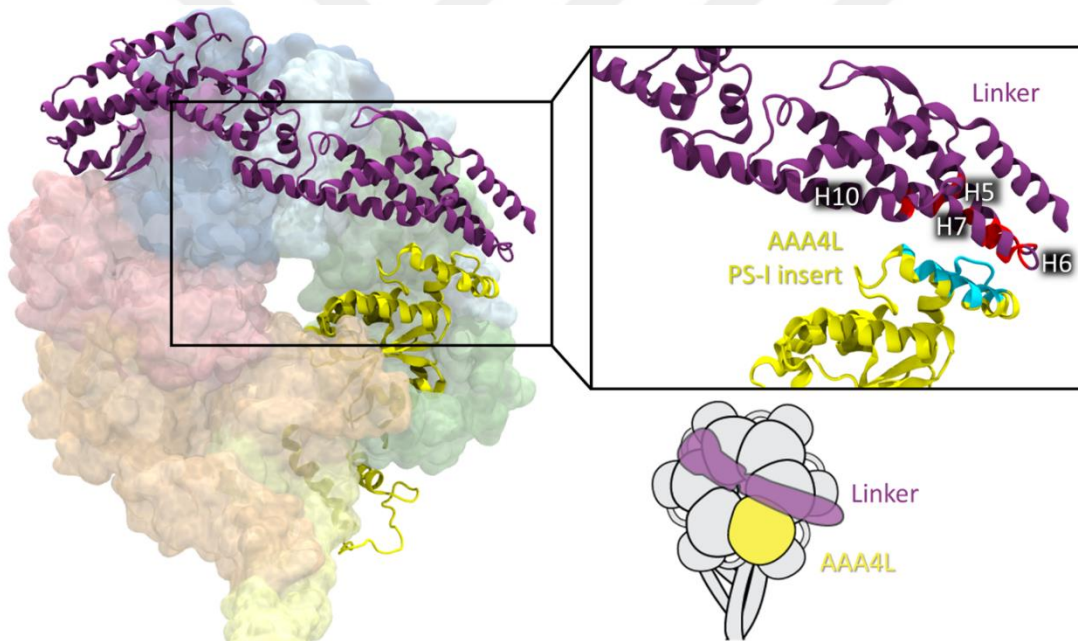


Figure 3.5 : Steric clash between the Link1-2 region of linker and AAA4L site. Left panel shows the AAA+ ring of the dynein obtained conformations after 80 ns of SMD-CMD simulations. Linker and AAA4, which are involved in the steric clash, are shown in cartoon representation whereas the remaining the remaining structural components are shown in surface representation. Right top panel shows the steric clash taking place between linker helices (H5-H7 and H10) and PS-I insert of AAA4L site. The right bottom panel shows the schematic illustration of the dynein AAA+ ring and linker during the steric clash. Large (L) and small (S) subdomains of AAA+ domains are shown separately in the schematic representation.

3.3 The Linker Movement During Priming Stroke is Energetically Favorable

In the previous section, the linker movement of the priming stroke was modeled using a subsequent SMD and CMD simulation. Then, UMD simulations were performed, which are started from end of the end conformations of first eight CMD simulations. UMD simulations were aimed to refine the transition pathway and explore the energetics of the linker swing movement in high resolution. Reaction coordinate ξ was selected as the RMSD of the bent linker structure to the straight linker conformation. End conformations of the CMD simulations were selected as equilibrium positions for harmonic restraints. Some of the regions of ξ were not widely sampled, for sampling there regions new UMD simulations were started from rarely sampled regions that overlap with these regions. 300 ns of UMD simulations were performed. Distribution of the UMD simulations are shown in Figure 3.6.

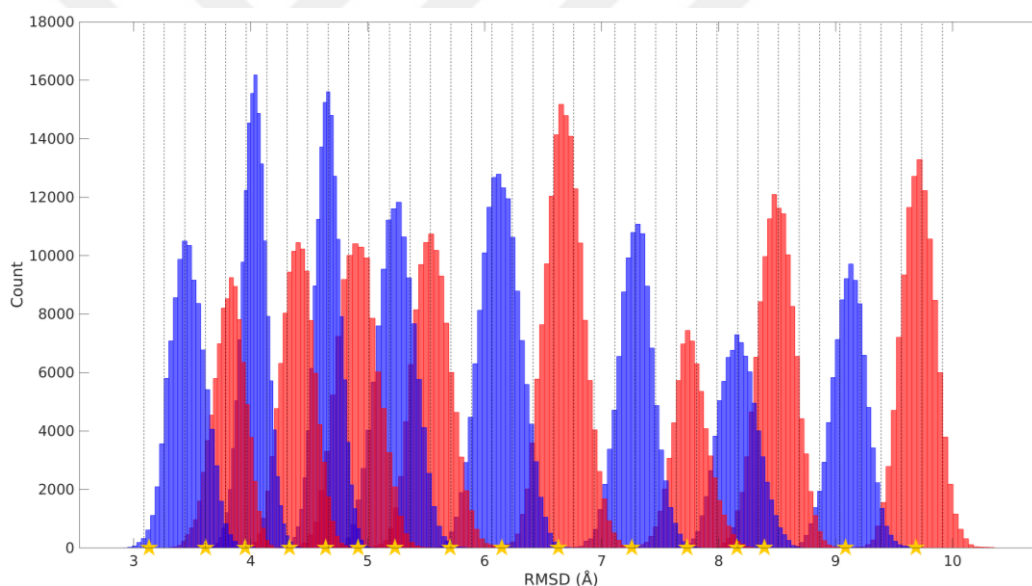


Figure 3.6 : Distribution of UMD simulations along the ξ . Dashed line indicates the gates, and yellow stars indicates center positions of the UMD.

3.4 Principal Component Analysis

All UMD simulations were combined into a single trajectory and PCA analysis were performed. PCA is an effective and proven method to investigate the most prominent motions a protein exhibits along a MD trajectory. PC1 and PC2 (Figure 3.7A-B) represent the most dominant two modes of motion in the combined UMD trajectory. PC1 mode of motion, which is the most dominant feature of the trajectory, moves H4, H5 and H7 towards the extended linker structure while slightly pointing towards the

hexameric ring. PC2, on the other hand, moves H4, H5 and H7 towards the extended linker structure and points slightly away from the hexameric ring. Conformations sampled in UMD were projected onto the PCs. The distributions of these projections are shown in Figure 3.7C.

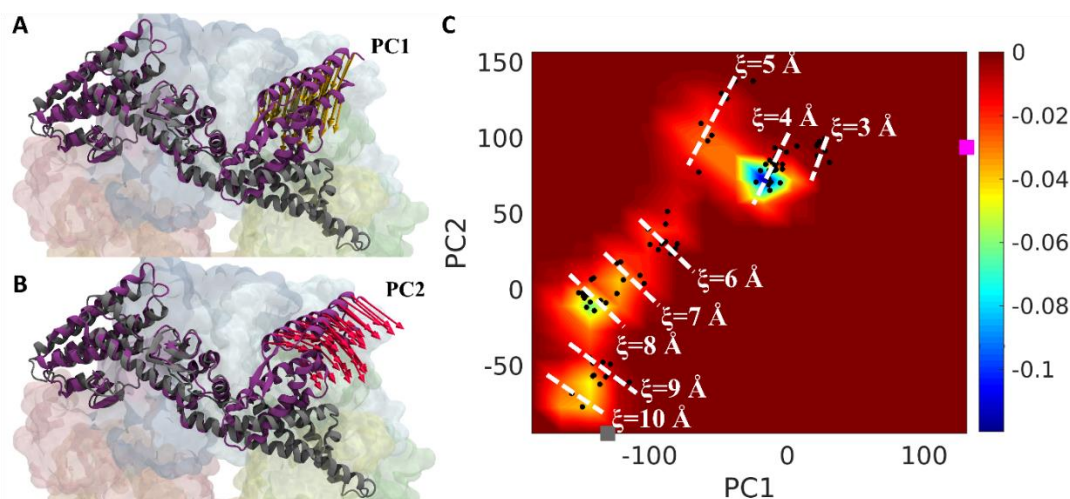


Figure 3.7 : Principal Component Analysis of UMD simulations. (A-B) The first two principal components of the complete UMD simulations data superimposed on a (TS3*: ATP, β , pre) conformation is shown. (C) Distribution of UMD simulations conformers along the first two principal components are shown. Dashed lines indicate the approximate position of the reaction coordinate on the distribution. (TS3: ADP.Pi, β , pre) and (TS5: ADP, α , post) crystal structures are shown with grey and magenta squares, respectively.

3.5 Free Energy Surface Calculation

To calculate the free energy surface for the linker movement during priming stroke, WHAM (Kumar et al., 1992) was applied using the UMD simulations data. Windows for dividing ξ was selected as 1 Å wide, in the range from 3 Å to 10 Å. Snapshots from the UMD simulations were clustered according to base on the windows. And, snapshot density of the UMD simulations are shown in Figure 3.7C. Snapshots that found in each ξ window and the magnitude of the guiding potential through the UMD simulations were identified. Free energy profile was established by using WHAM (Eqs. 6-9) as a function of ξ and free energy profile is shown in Figure 3.8. Decreasing free energy profile was observed from 3 Å to 10 Å. Free energy difference between of $\Delta\Phi = \Phi(10 \text{ \AA}) - \Phi(3 \text{ \AA}) = -40.4 \text{ kJ/mol}$. It shows that linker movement during the priming stroke is energetically favorable.

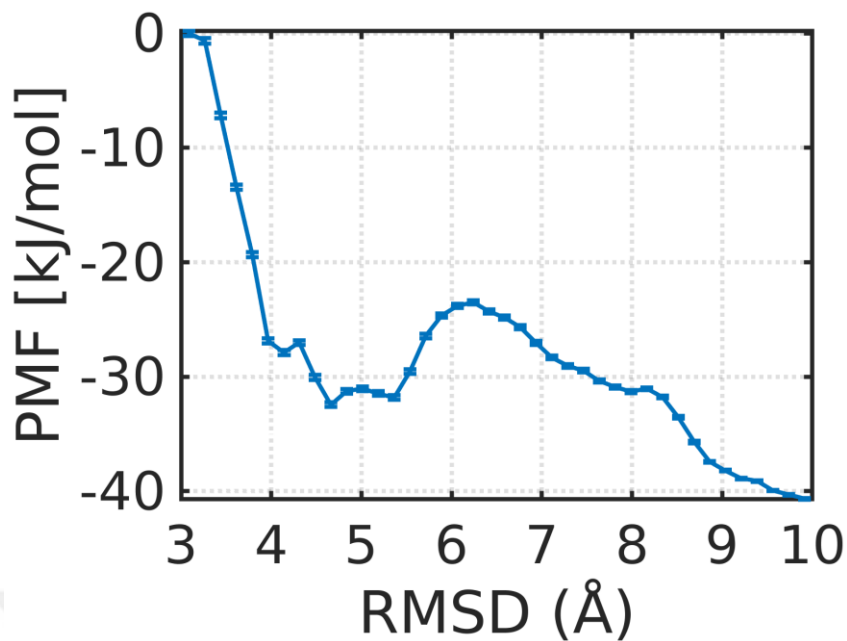


Figure 3.8 : Free energy profile along the reaction coordinate with error bar of the linker priming movement. Free energy profile as a function of the RMSD between the extended linker structure and the linker conformations sampled during UMD simulations.

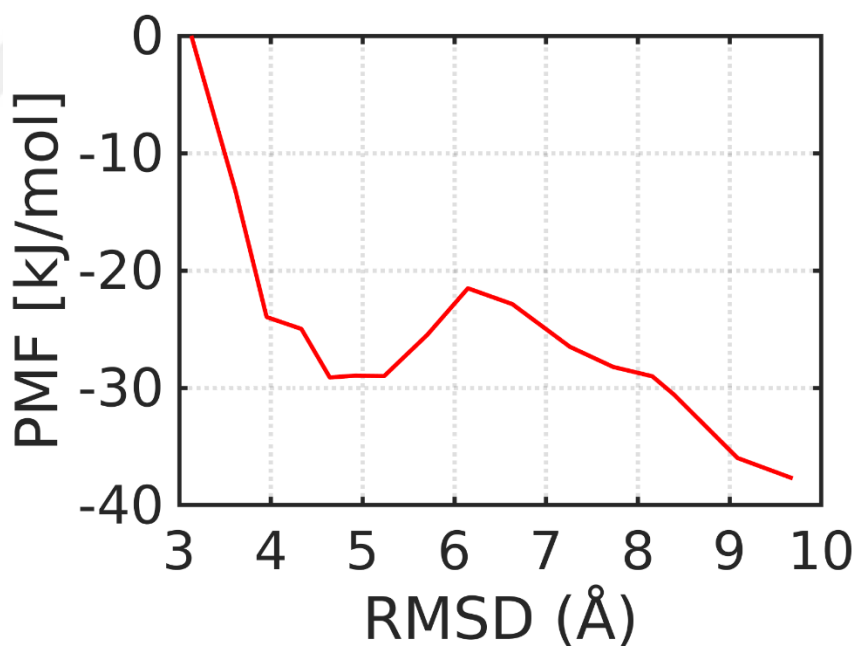


Figure 3.9 : Free energy profile error estimation with Bootstrapping analysis. In this graph show that PMF construct from randomly sampled values according to the obtained weighted histograms.

3.6 During Priming Stroke the Linker Interdomain Salt Bridges Switch from AAA4 to AAA3

Salt bridges in the dynein structure may be grouped into two types: i) those existing independently of the transition and reinforcing the structure, and ii) salt bridges that forms or breaks during conformational transitions of the mechanochemical cycle. Type II salt bridges are expected to strongly contribute to, or even facilitate, the stability of states along the mechanochemical cycle of dynein. Investigation of type 2 salt bridges between the linker and hexameric ring in the conformers generated by the MD simulations show a distinct pattern of interdomain salt bridges for the extended and bent forms of the linker. For the straight linker ($\xi = 3 \text{ \AA}$), the type II salt bridges between Link1-2 and the hexameric ring are predominantly with AAA4, which are listed as follows: K1296 (H5) - E2393 (AAA3), R1306 (H5) - E2742 (AAA4), K1313 (H5) - E2745 (AAA4), D1314 (H5) - K2349 (AAA3), K1319 (H6) - D2753 (AAA4), and E1322 (H7) - K2752 (AAA4). For the bent linker ($\xi = 10 \text{ \AA}$), on the other hand, Link1-2 formed the following interdomain type II salt bridge with AAA3; E1337(H7)-R2344(AAA3). Additionally, the bent linker formed intradomain type II salt bridges with the linker hinge, E1364 (H8) - K1413 (H10), and with Link3-4, K1348 (H7) - D1435 (H12). Thus, in total the straight linker formed 6 type II salt bridges while the bent linker formed only 3 type II salt bridges. The locations of the type II salt bridges for the straight and bent linker conformations are shown in Figure 3.10.

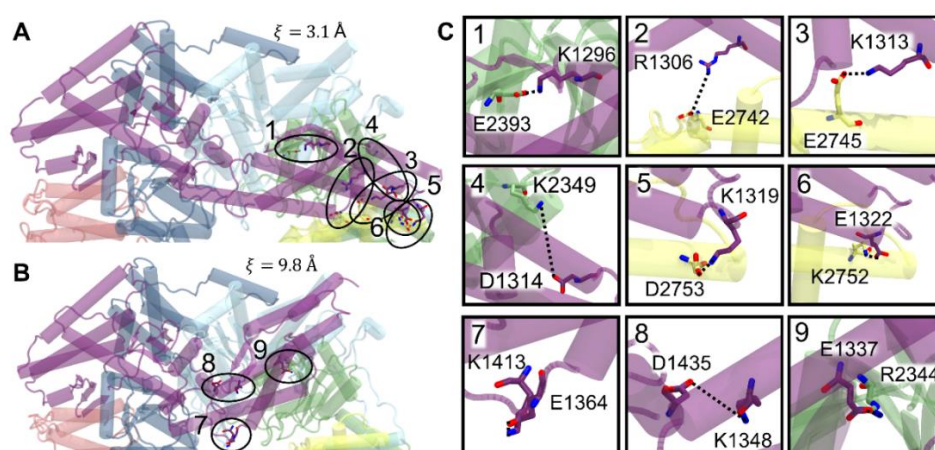


Figure 3.10 : Location of salt bridges broken and formed throughout the linker movement during priming stroke. (A) Type II interdomain salt bridges between Link1-2 and AAA3-4 of the straight linker are shown. (B) The type 2 interdomain salt bridge with AAA3 and the intradomain salt bridges of the bent linker are shown. (C) Salt bridges in the left panels are numbered and each salt bridge is magnified in the right panel.

Based on the MD simulations data we predict that the linker movement during the priming stroke from $\xi = 3 \text{ \AA}$ to $\xi = 10 \text{ \AA}$ comprises in a net change of 3 broken salt bridges. Salt bridges can provide 12–20 kJ/mol of energy to the protein stability (Makhatadze, Loladze, Ermolenko, Chen, & Thomas, 2003). Thus, the net change of 3 salt bridges is expected to release an energy of 36-60 kJ/mol, which will contribute only partially to the free energy released during the linker movement from $\xi = 3 \text{ \AA}$ to $\xi = 10 \text{ \AA}$. As indicated earlier, conformations sampled in the UMD simulations were clustered based on their reaction coordinates. For each conformation the distances between the closest nitrogens and oxygens belonging to the pairs of salt bridge forming amino acids were evaluated. Average N-O distances for these pairs were calculated at each window/cluster along the reaction coordinate. A cutoff distance of 6 \AA (Gur, Madura, & Bahar, 2013) was used as a criteria whether a salt bridge is present. If the cluster average N-O distance between a salt bridge forming pair was less than the cutoff distance, then the type II salt bridge was deemed to be present at that window along ξ . Based on these criteria, the evolution of salt bridges along the reaction coordinate were determined and depicted in Figure 3.11.

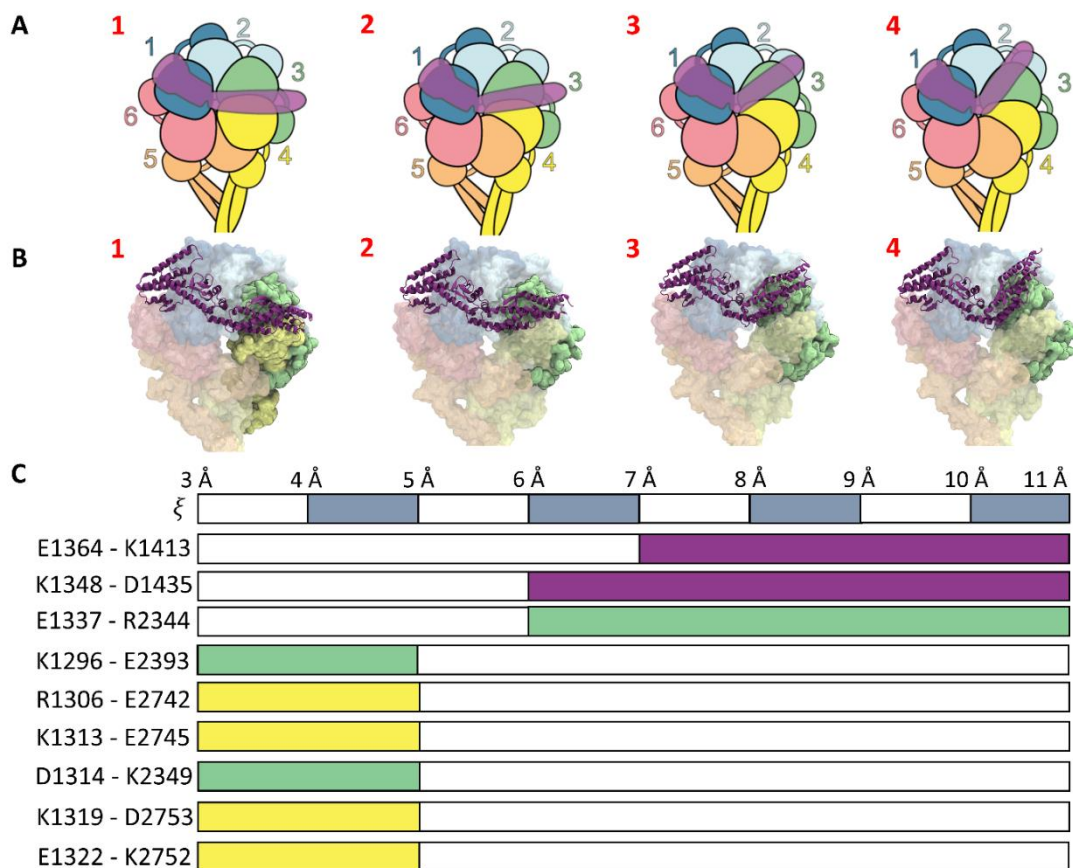


Figure 3.11 : Evolution of salt bridges during the linker movement of the priming stroke (A) Illustrative representation of the linker position with respect to the AAA+ ring along the reaction coordinate. (B) Representative conformations sampled from UMD simulations along the reaction coordinate. (C) Presence of Type II salt bridges along the reaction coordinate. White colors indicate that the salt bridges are not present at that specific point along the reaction coordinate. The coloring for the salt bridge indicates the domain with which Link1-2 is forming a salt bridge. Thus, magenta indicates intradomain salt bridges. Green and yellow indicate interdomain salt bridges between the linker and AAA3 and AAA4, respectively

4. CONCLUSIONS AND FUTURE RESEARCH

In this thesis, the structural mechanism and energetics of the priming stroke, transition of the linker from TS2 to TS3, of the DHC mechanochemical cycle have been obtained in detail by using SMD, conventional MD and UMD simulations. The transition pathway of the linker in the ATP bound form of DHC have been modeled. According to results, the linker is able to sample the region spanning AAA4/AAA3 to AAA3/AAA2 without coming across a steric clash during the transition. Schmidt et al.(2015) reported that ATP binding should cause a structural change in the catalytic ring so that a steric clash occurs between AAA4 and the linker, which they proposed to potentially force the linker to move towards its bent form. The extent of such an induced movement, however, is not known in literature. The MD simulation results presented in the thesis suggest that the structural change of the catalytic ring induced by ATP binding forces the linker to move from AAA5/AAA4 to AAA4/AAA3. Moreover, UMD simulations were performed to extensively sample the transition pathway and explore the energetics of the linker conformational transition. The free energy difference between the straight and bent forms of the linker is ~ -40 kJ/mol. The results show that the priming stroke is an energetically favorable process. Thus, it does not require an external energy input. This is a significant result, as it indicates that ATP hydrolysis can supply enough energy to move the linker in the reverse direction of the priming stroke (62 kJ/mol).

The priming stroke (TS2 \rightarrow TS3) takes place in the MT unbound form of DHC, and the power stroke (TS4 \rightarrow TS5), takes place in the MT bound form DHC. As MT binding is known to affect the stalk registry, which in turn affects the catalytic ring structure, it is possible that the order of structural changes observed in the catalytic ring and the linker might not be the same for the power stroke and priming stroke. To obtain detailed information about the power stroke mechanism, dynein structure has to be docked to the MT. Subsequently, a procedure similar to the procedure performed in this thesis can be potentially applied to the DHC-MT system to model the detailed mechanism and energetics of the power stroke.



REFERENCES

- Barakat-Walter, I., & Riederer, B.** (1996). Triiodothyronine and nerve growth factor are required to induce cytoplasmic dynein expression in rat dorsal root ganglion cultures. *Developmental brain research*, 96(1-2), 109-119.
- Best, R. B., Zhu, X., Shim, J., Lopes, P. E., Mittal, J., Feig, M., & MacKerell Jr, A. D.** (2012). Optimization of the additive CHARMM all-atom protein force field targeting improved sampling of the backbone ϕ , ψ and side-chain χ_1 and χ_2 dihedral angles. *Journal of chemical theory and computation*, 8(9), 3257-3273.
- Bhabha, G., Cheng, H.-C., Zhang, N., Moeller, A., Liao, M., Speir, J. A., . . . Vale, R. D.** (2014). Allosteric communication in the dynein motor domain. *Cell*, 159(4), 857-868.
- Blocker, A., Severin, F. F., Burkhardt, J. K., Bingham, J. B., Yu, H., Olivo, J.-C., . . . Griffiths, G.** (1997). Molecular requirements for bi-directional movement of phagosomes along microtubules. *The Journal of cell biology*, 137(1), 113-129.
- Brady, S. T.** (1985). A novel brain ATPase with properties expected for the fast axonal transport motor. *Nature*, 317(6032), 73.
- Bullock, S. L., Nicol, A., Gross, S. P., & Zicha, D.** (2006). Guidance of bidirectional motor complexes by mRNA cargoes through control of dynein number and activity. *Current Biology*, 16(14), 1447-1452.
- Burgess, S. A., Walker, M. L., Sakakibara, H., Knight, P. J., & Oiwa, K.** (2003). Dynein structure and power stroke. *Nature*, 421(6924), 715.
- Can, S., Lacey, S., Gur, M., Carter, A. P., & Yildiz, A.** (2019). Directionality of dynein is controlled by the angle and length of its stalk. *Nature*, 566(7744), 407.
- Cheng, H. H., Liu, S. H., Lee, H. C., Lin, Y. S., Huang, Z. H., Hsu, C. I., . . . Chang, Y. C.** (2006). Heavy chain of cytoplasmic dynein is a major component of the postsynaptic density fraction. *Journal of neuroscience research*, 84(2), 244-254.
- Cochran, J.** (2015). Kinesin motor enzymology: chemistry, structure, and physics of nanoscale molecular machines. *Biophysical reviews*, 7(3), 269-299.
- Dagenbach, E. M., & Endow, S. A.** (2004). A new kinesin tree. *Journal of cell science*, 117(1), 3-7.
- Dodding, M. P., & Way, M.** (2011). Coupling viruses to dynein and kinesin-1. *The EMBO journal*, 30(17), 3527-3539.
- Driskell, O. J., Mironov, A., Allan, V. J., & Woodman, P. G.** (2007). Dynein is required for receptor sorting and the morphogenesis of early endosomes. *Nature cell biology*, 9(1), 113.
- El-Kadi, A. M., Soura, V., & Hafezparast, M.** (2007). Defective axonal transport in motor neuron disease. *Journal of neuroscience research*, 85(12), 2557-2566.

- Engels, M., Jacoby, E., Krüger, P., Schlitter, J., & Wollmer, A.** (1992). The T \rightleftharpoons R structural transition of insulin; pathways suggested by targeted energy minimization. *Protein Engineering, Design and Selection*, 5(7), 669-677.
- Eschbach, J., & Dupuis, L.** (2011). Cytoplasmic dynein in neurodegeneration. *Pharmacology & therapeutics*, 130(3), 348-363.
- Gaetz, J., & Kapoor, T. M.** (2004). Dynein/dynactin regulate metaphase spindle length by targeting depolymerizing activities to spindle poles. *The Journal of cell biology*, 166(4), 465-471.
- Gee, M. A., Heuser, J. E., & Vallee, R. B.** (1997). An extended microtubule-binding structure within the dynein motor domain. *Nature*, 390(6660), 636.
- Gibbons, I.** (1963). Studies on the protein components of cilia from *Tetrahymena pyriformis*. *Proceedings of the National Academy of Sciences of the United States of America*, 50(5), 1002.
- Gross, S. P., Tuma, M. C., Deacon, S. W., Serpinskaya, A. S., Reilein, A. R., & Gelfand, V. I.** (2002). Interactions and regulation of molecular motors in *Xenopus melanophores*. *The Journal of cell biology*, 156(5), 855-865.
- Gross, S. P., Welte, M. A., Block, S. M., & Wieschaus, E. F.** (2000). Dynein-mediated cargo transport in vivo: a switch controls travel distance. *The Journal of cell biology*, 148(5), 945-956.
- Grotjahn, D. A., & Lander, G. C.** (2019). Setting the dynein motor in motion: New insights from electron tomography. *Journal of Biological Chemistry*, 294(36), 13202-13217.
- Gur, M., Madura, J. D., & Bahar, I.** (2013). Global transitions of proteins explored by a multiscale hybrid methodology: application to adenylate kinase. *Biophys J*, 105(7), 1643-1652. doi:10.1016/j.bpj.2013.07.058
- Hafezparast, M., Klocke, R., Ruhrberg, C., Marquardt, A., Ahmad-Annuar, A., Bowen, S., . . . Nicholson, S.** (2003). Mutations in dynein link motor neuron degeneration to defects in retrograde transport. *Science*, 300(5620), 808-812.
- Harrell, J. M., Murphy, P. J., Morishima, Y., Chen, H., Mansfield, J. F., Galigniana, M. D., & Pratt, W. B.** (2004). Evidence for glucocorticoid receptor transport on microtubules by dynein. *Journal of Biological Chemistry*, 279(52), 54647-54654.
- Heald, R., Tournebise, R., Blank, T., Sandaltzopoulos, R., Becker, P., Hyman, A., & Karsenti, E.** (1996). Self-organization of microtubules into bipolar spindles around artificial chromosomes in *Xenopus* egg extracts. *Nature*, 382(6590), 420.
- Hirokawa, N.** (1998). Kinesin and dynein superfamily proteins and the mechanism of organelle transport. *Science*, 279(5350), 519-526.
- Hirokawa, N., Noda, Y., Tanaka, Y., & Niwa, S.** (2009). Kinesin superfamily motor proteins and intracellular transport. *Nature reviews Molecular cell biology*, 10(10), 682.
- Holzbaur, E., & Vallee, R.** (1994). Dyneins: molecular structure and cellular function. *Annual review of cell biology*, 10(1), 339-372.
- Höök, P., & Vallee, R. B.** (2006). The dynein family at a glance. *Journal of cell science*, 119(21), 4369-4371.
- Howell, B., McEwen, B., Canman, J., Hoffman, D., Farrar, E., Rieder, C., & Salmon, E.** (2001). Cytoplasmic dynein/dynactin drives kinetochore protein transport to the spindle poles and has a role in mitotic spindle checkpoint inactivation. *J Cell Biol*, 155(7), 1159-1172.

- Humphrey, W., Dalke, A., & Schulten, K.** (1996). VMD: visual molecular dynamics. *Journal of molecular graphics*, 14(1), 33-38.
- Isralewitz, B., Gao, M., & Schulten, K.** (2001). Steered molecular dynamics and mechanical functions of proteins. *Current opinion in structural biology*, 11(2), 224-230.
- Johnston, J. A., Illing, M. E., & Kopito, R. R.** (2002). Cytoplasmic dynein/dynactin mediates the assembly of aggresomes. *Cell motility and the cytoskeleton*, 53(1), 26-38.
- Jordens, I., Fernandez-Borja, M., Marsman, M., Dusseljee, S., Janssen, L., Calafat, J., . . . Neefjes, J.** (2001). The Rab7 effector protein RILP controls lysosomal transport by inducing the recruitment of dynein-dynactin motors. *Current Biology*, 11(21), 1680-1685.
- Kon, T., Imamula, K., Roberts, A. J., Ohkura, R., Knight, P. J., Gibbons, I., . . . Sutoh, K.** (2009). Helix sliding in the stalk coiled coil of dynein couples ATPase and microtubule binding. *Nature structural & molecular biology*, 16(3), 325.
- Kon, T., Nishiura, M., Ohkura, R., Toyoshima, Y. Y., & Sutoh, K.** (2004). Distinct functions of nucleotide-binding/hydrolysis sites in the four AAA modules of cytoplasmic dynein. *Biochemistry*, 43(35), 11266-11274.
- Kon, T., Oyama, T., Shimo-Kon, R., Imamula, K., Shima, T., Sutoh, K., & Kurisu, G.** (2012). The 2.8 Å crystal structure of the dynein motor domain. *Nature*, 484(7394), 345.
- Kumar, S., Rosenberg, J. M., Bouzida, D., Swendsen, R. H., & Kollman, P. A.** (1992). The weighted histogram analysis method for free-energy calculations on biomolecules. I. The method. *Journal of computational chemistry*, 13(8), 1011-1021.
- Kural, C., Kim, H., Syed, S., Goshima, G., Gelfand, V. I., & Selvin, P. R.** (2005). Kinesin and dynein move a peroxisome in vivo: a tug-of-war or coordinated movement? *Science*, 308(5727), 1469-1472.
- Makhatadze, G. I., Loladze, V. V., Ermolenko, D. N., Chen, X., & Thomas, S. T.** (2003). Contribution of surface salt bridges to protein stability: guidelines for protein engineering. *Journal of molecular biology*, 327(5), 1135-1148.
- Matsunaga, Y.** (2015, June 19, 2019). MDToolBox. Retrieved from <https://mdtoolbox.readthedocs.io>
- Maupin, P., Phillips, C. L., Adelstein, R. S., & Pollard, T. D.** (1994). Differential localization of myosin-II isozymes in human cultured cells and blood cells. *Journal of cell science*, 107(11), 3077-3090.
- Neuwald, A. F., Aravind, L., Spouge, J. L., & Koonin, E. V.** (1999). AAA+: A class of chaperone-like ATPases associated with the assembly, operation, and disassembly of protein complexes. *Genome research*, 9(1), 27-43.
- O'halloran, T. J., Ravid, S., & Spudich, J. A.** (1990). Expression of Dictyostelium myosin tail segments in Escherichia coli: domains required for assembly and phosphorylation. *The Journal of cell biology*, 110(1), 63-70.
- Odronitz, F., & Kollmar, M.** (2007). Drawing the tree of eukaryotic life based on the analysis of 2,269 manually annotated myosins from 328 species. *Genome biology*, 8(9), R196.
- Ogawa, K.** (1991). Four ATP-binding sites in the midregion of the β heavy chain of dynein. *Nature*, 352(6336), 643.

- Paschal, B. M., Shpetner, H. S., & Vallee, R. B.** (1987). MAP 1C is a microtubule-activated ATPase which translocates microtubules in vitro and has dynein-like properties. *The Journal of cell biology*, 105(3), 1273-1282.
- Paschal, B. M., & Vallee, R. B.** (1987). Retrograde transport by the microtubule-associated protein MAP 1C. *Nature*, 330(6144), 181.
- Pazour, G. J., Dickert, B. L., & Witman, G. B.** (1999). The DHC1b (DHC2) isoform of cytoplasmic dynein is required for flagellar assembly. *The Journal of cell biology*, 144(3), 473-481.
- Perrone, C. A., Tritchler, D., Taulman, P., Bower, R., Yoder, B. K., & Porter, M. E.** (2003). A novel dynein light intermediate chain colocalizes with the retrograde motor for intraflagellar transport at sites of axoneme assembly in *Chlamydomonas* and mammalian cells. *Molecular biology of the cell*, 14(5), 2041-2056.
- Phillips, J., Isgro, T., Sotomayor, M., & Villa, E.** (2003). NAMD TUTORIAL.
- Phillips, J. C., Braun, R., Wang, W., Gumbart, J., Tajkhorshid, E., Villa, E., . . . Schulten, K.** (2005). Scalable molecular dynamics with NAMD. *Journal of computational chemistry*, 26(16), 1781-1802.
- Pilling, A. D., Horiuchi, D., Lively, C. M., & Saxton, W. M.** (2006). Kinesin-1 and Dynein are the primary motors for fast transport of mitochondria in *Drosophila* motor axons. *Molecular biology of the cell*, 17(4), 2057-2068.
- Porter, M. E., Bower, R., Knott, J. A., Byrd, P., & Dentler, W.** (1999). Cytoplasmic dynein heavy chain 1b is required for flagellar assembly in *Chlamydomonas*. *Molecular biology of the cell*, 10(3), 693-712.
- Presley, J. F., Cole, N. B., Schroer, T. A., Hirschberg, K., Zaal, K. J., & Lippincott-Schwartz, J.** (1997). ER-to-Golgi transport visualized in living cells. *Nature*, 389(6646), 81.
- Roberts, A. J., Kon, T., Knight, P. J., Sutoh, K., & Burgess, S. A.** (2013). Functions and mechanics of dynein motor proteins. *Nature reviews Molecular cell biology*, 14(11), 713-726.
- Roberts, A. J., Numata, N., Walker, M. L., Kato, Y. S., Malkova, B., Kon, T., . . . Sutoh, K.** (2009). AAA+ Ring and linker swing mechanism in the dynein motor. *Cell*, 136(3), 485-495.
- Sasaki, S., Shionoya, A., Ishida, M., Gambello, M. J., Yingling, J., Wynshaw-Boris, A., & Hirotsune, S.** (2000). A LIS1/NUDEL/cytoplasmic dynein heavy chain complex in the developing and adult nervous system. *Neuron*, 28(3), 681-696.
- Schlitter, J., Engels, M., & Krüger, P.** (1994). Targeted molecular dynamics: a new approach for searching pathways of conformational transitions. *Journal of molecular graphics*, 12(2), 84-89.
- Schliwa, M.** (1999). Myosin steps backwards. *Nature*, 401(6752), 431.
- Schmidt, H., Gleave, E. S., & Carter, A. P.** (2012). Insights into dynein motor domain function from a 3.3-Å crystal structure. *Nature structural & molecular biology*, 19(5), 492.
- Schmidt, H., Zalyte, R., Urnavicius, L., & Carter, A. P.** (2015). Structure of human cytoplasmic dynein-2 primed for its power stroke. *Nature*, 518(7539), 435.
- Schnapp, B. J., & Reese, T. S.** (1989). Dynein is the motor for retrograde axonal transport of organelles. *Proceedings of the National Academy of Sciences*, 86(5), 1548-1552.

- Soo, K. Y., Farg, M., & Atkin, J. D.** (2011). Molecular motor proteins and amyotrophic lateral sclerosis. *International journal of molecular sciences*, *12*(12), 9057-9082.
- Souaille, M., & Roux, B.** (2001). Extension to the weighted histogram analysis method: combining umbrella sampling with free energy calculations. *Computer physics communications*, *135*(1), 40-57.
- Syamaladevi, D. P., Spudich, J. A., & Sowdhamini, R.** (2012). Structural and functional insights on the Myosin superfamily. *Bioinformatics and biology insights*, *6*, BBI.S8451.
- The MathWorks, I.** (2019). MATLAB (Version 2019a). Natick, Massachusetts, United States: The MathWorks, Inc.
- Thompson, R. F., & Langford, G. M.** (2002). Myosin superfamily evolutionary history. *The Anatomical Record: An Official Publication of the American Association of Anatomists*, *268*(3), 276-289.
- Vale, R. D.** (2000). AAA proteins: lords of the ring. *J Cell Biol*, *150*(1), F13-F20.
- Vale, R. D., Reese, T. S., & Sheetz, M. P.** (1985). Identification of a novel force-generating protein, kinesin, involved in microtubule-based motility. *Cell*, *42*(1), 39-50.
- Vallee, R. B., & Sheetz, M. P.** (1996). Targeting of motor proteins. *Science*, *271*(5255), 1539-1544.
- Wells, A. L., Lin, A. W., Chen, L.-Q., Safer, D., Cain, S. M., Hasson, T., . . . Sweeney, H. L.** (1999). Myosin VI is an actin-based motor that moves backwards. *Nature*, *401*(6752), 505.
- Yamada, M., Tanaka-Takiguchi, Y., Hayashi, M., Nishina, M., & Goshima, G.** (2017). Multiple kinesin-14 family members drive microtubule minus end-directed transport in plant cells. *J Cell Biol*, *216*(6), 1705-1714.



APPENDICES

APPENDIX A: Sequence alignment of the Dynein

		4RH7 (ADP.Vi)	3VKG (ADP)	
DYHC2_HUMAN	1079	SAKLIKEKKI----	EFDDLEVTRKKLVDDCHHFRLEEPNFSLASSISKDIESCAQIWAFY	1134
DYHC_DICDI	1346	TLKIFEGRLIRLREESDRLSKAKQAL-DLTDTTGSSSSDQDRLVPEEEIQDLKAVWVVEL		1404
DYHC_YEAST	1186	ILEFFNESITKLRKKMHSAVAAAAMKL-LI-----PVLNDQLTHVVEEVKTYDLVWRSI		1238
DYHC2_HUMAN	1135	EEFQQGFQEMANEDWITFRKT--YLFEEFLMNWHDRLRKVEEHSVMTVKLQSEVDKYKI		1192
DYHC_DICDI	1405	SNTWQEI DSLKETAWSAIIPRKVRKSLDTLQKLNLPNRIR-QYSAFDHAQNLIKIYLK		1463
DYHC_YEAST	1239	<u>KNLWEDVQRTFETFPWCRVDVLLQLQSDLANFLRRADELPRAVK-QFEMYKSLFSQVNMLTS</u>		1297
DYHC2_HUMAN	1193	VIPIILKYVRGEHLSPDHWLDFRLLGLPRGTS--LEK--LLFGDLLRVADTIVAKAADLK		1248
DYHC_DICDI	1464	GNAIITDLHSEAIKDRHWKILKKRLNTNWIITE-----LTLGSIWD--SDLARNENIYR		1515
DYHC_YEAST	1298	<u>VNKILVELKDGALKPRHWNMIFRDIQGRQIQKNLLDKLEFSLKDVMMV--LNLTLNEILLT</u>		1355
		4AKG (APO)		
DYHC2_HUMAN	1249	DLNSRAQGEVTIREALRELDLWGVGAVFTLIDYEDSQSRTMKLIKDWKDIVNQVGDNRCL		1308
DYHC_DICDI	1516	EVITAAQGEI ALEEF LKGVREFWTTLELDLVNY----QRKCKLVRGWDDLFNKLAEHLNS		1571
DYHC_YEAST	1356	KIIERAQKEFVIEKSLNRIKKFEWKEAQYEVIEH----SSGLKLVREWDVLEOACKEDLEE		1411
DYHC2_HUMAN	1309	LQSLKDSPYKGFEDKVS IWERKLAELDEYLQNLNHIQRKWVYLEPIFGRG----ALPK		1363
DYHC_DICDI	1572	ISAMKMSPYKVFEEANHWDDRLNKNVRSLLDVWIDVQRRWVYLEGIFSGSGDINQLLPA		1631
DYHC_YEAST	1412	<u>LVSMKASNYYKIFEQDCLDLESKLTKLSEIQVNWVEVQFYWLDLYGILGENLDIQNFIPL</u>		1471
DYHC2_HUMAN	1364	EQTRFNRVDEDFRSIMTDIKKDNRVTTLTTHAGIRNSLLTILDQLQRCQKSLNEFLEEKR		1423
DYHC_DICDI	1632	ESTRFKINSSEFIAILKKVSGAPLILEVLAIERIQQTMRSDLLGKQKALGEYLERQR		1691
DYHC_YEAST	1472	<u>ETSKFKSLTSEYKMITTRAFOLDTTELEVIHIPNFDTTLKLTIDSLKMIKSSSLTFLERQR</u>		1531
DYHC2_HUMAN	1424	SAFPRFYFIGDDLLEILGQSTNPVSIQSHLKKLFAGINSVCFDEKSKHITAMKSLEGEV		1483
DYHC_DICDI	1692	SAFARFYFVGDEDLLEIIGNSKDIIKIQKHFRKMFAGLANLTLDDDEKTTIIGMSSAEGET		1751
DYHC_YEAST	1532	<u>RQFPRFYFLGNDLLKII GSGKHHQVSKFMKMFSGSIESIFLE--DFITGVRSVEGEV</u>		1589
DYHC2_HUMAN	1484	VPFKNKVPLSNN--VETWLNDLALEMKTLEQLLKECVTTGR-----SSQGAVDPSLFP		1535
DYHC_DICDI	1752	VTFKKPI SIANGPKIHEWLTMVSEMKSTLATLSESLQHFNOVDVNDHYSKYSEWVDNYP		1811
DYHC_YEAST	1590	<u>LNLNEKIELKDSIQAEWLNILDTEIKLSVFTQFRDCLGQL-----KDGTDIEVVVSKYI</u>		1644
DYHC2_HUMAN	1536	SQILCLAEQIKFTEDVENAIKDHS LHQIETQLV-NKLEQYTN--IDTSSDPGNTESGIL		1592
DYHC_DICDI	1812	TQLVLLTSQIVWSTQVDQALGGGTLQQSKIQEQLQSI EQTTQMI LNNLADSVLQDLSAQK		1871
DYHC_YEAST	1645	<u>FQAILLSAQVMWTELVEKCLQTNQFSKYW-----KE----VDMKIKGLLDK-LNKSSDNV</u>		1694
DYHC2_HUMAN	1593	ELKALKALILDIIHNIDVVKQLNQIQVHTT-EDWAWKKQLRFYMKSDH----TCCVQMV		1646
DYHC_DICDI	1872	RKKFEHLITELVHQRDVVRQLQKCKNLTGNKDFDWLYHMRYYYDATQENVLHKLVIHMAN		1931
DYHC_YEAST	1695	<u>KKKIEALLVEYLHFNNVIGQLKNCSTKEE-ARLLWAKVQKFYOKNDTLDDLNSVFISQSG</u>		1753
DYHC2_HUMAN	1647	<u>SEFQYTYEYQGNASKLVYTP</u> LTDKCYLTLTQAMKMLGGNPYGPA GTGKTESVKALGGLL		1706
DYHC_DICDI	1932	ATFFYGF EYLGIGERLVQTP LTRCYLTLTQALESRMGGNPFPGAGTGTETVKALGSQL		1991
DYHC_YEAST	1754	<u>YLLQYKFEYIGIPERLIYTP</u> LLLI GFATLTD SLHOKYGGCFPGAGTGTETVKAFGQNL		1813

DYHC2_HUMAN	2258	LTLFVIQTPDMQRGLDYFKPWLSDDTKQPFILVGPPEGCGKGMLLRYAFSQLRSTQIATVH	2317
DYHC_DICDI	2643	SPDVVIPTVDTTRHVDVLHAWLSE--HRPLILCGPPGSGKMTLTSTLRAFPDFEVVSLN	2700
DYHC_YEAST	2387	RPDIVIPTIDTIKHEKIFYDLLNS--KRGIIICGPPGSGKTMIMNNALRNSSLYDVVGIN	2444
		AAA3L	
DYHC2_HUMAN	2318	CSAQTTSRHLLQKLSQTCMVISSTNTGRVYRPK--DCERLVLYLKDINLPKLDKWTSTLV	2375
DYHC_DICDI	2701	FSSATTPPELLLKTFDHHCYKRTPSGETVLRPTQLGKWLWVFCDEINLPSTDKYGTQRVI	2760
DYHC_YEAST	2445	FSKDTTTEHILSALHRHTNYVTTSKGLTLLPKS-DIKNLVLCFEINLPKLDKYGSQNVV	2503
		H2-S3 insert	
DYHC2_HUMAN	2376	AFLQQVLTYYGGFYDE-NLEWVGLENIQIVASMSAGGRLGRHKLTTRFTSIVRLCSIDYPE	2434
DYHC_DICDI	2761	TFIRQMVKEKGGFWRTSDHTWIKLDKIQFVGACNPPTDAGRVLTHRFLRHAPILLVDFFS	2820
DYHC_YEAST	2504	LFLROLMEKQGGFWKTPENKQVTERIHIIVGACNPPTDPGRIPMSERFTRHAAILLYLGYP	2563
		PS-I insert	
DYHC2_HUMAN	2435	REQLQTIYGAYLEPVLHKNLKNHSIWGSSSKIYLLAGSMVQVYEQVRAKFTVDDYSHYFF	2494
DYHC_DICDI	2821	TSSLTQIYGTFNRAIMKLLPNL-----RSFADNLTAMVEFYSESQKRFTPDIQAHYIY	2874
DYHC_YEAST	2564	GKLSQIYEIYYKAIKFLVPEF-----RSYTEFFARASVHLYNECKARYSTGLQSHYLF	2617
		AAA3S	
DYHC2_HUMAN	2495	TPCILTQVWLGLFRYDLEGGSSNHPLDYVLEIVAYEARRLFDRDKIVGAKELHFLDIILTS	2554
DYHC_DICDI	2875	SPRELSRWDRALEAIQTM--DGCTLEGLVRLWAHEALRLFQDRLVTEEEKWTDKKIDE	2932
DYHC_YEAST	2618	SPRELTRLRVGVYTAINTG--PRQTLRSLIRLWAYEAWRIFADRLVGVKEKNSFEQLLYE	2675
DYHC2_HUMAN	2555	VFQGDWGSIDLDNMSDS--FYVTWGARHNSGARAAPGQPLPPHGKPLGKLNSTDLKDVIK	2612
DYHC_DICDI	2933	VALKHFPVSNLDAL-KRPILYSNWL-----TKDYQPVNRSDLREYVK	2973
DYHC_YEAST	2676	TVDKYLPNQDLGNISSTSLFSGLL-----SLDFKEVNKTDLVNFIE	2717
DYHC2_HUMAN	2613	KGLIHYGRDNQNLDILLFHEVLEYMSRIDRVLSFPGGSLLAGRSGVGRRTITSLVSHMH	2672
DYHC_DICDI	2974	ARLKVFEHEELDVPVLFNEVLHDHILRIDRVFRQPQGHALLIGVSGGKSVLSRFVAVMN	3033
DYHC_YEAST	2718	ERFKTFCDEELEVPMVIHESMVDHILRIDRALKQVQGHMMLIGASRTGKTIILTRFVAVLN	2777
		AAA4L	
DYHC2_HUMAN	2673	GAVLFSPKISRGYELKQFKNDLKHVLQLAGIEAQVVLLEEDYQFVHPTFLEMINSLLSS	2732
DYHC_DICDI	3034	GLSIYTIKVNNNYKSSDFDDDLRMLLRAGCKEEKICIFDES NVLESSFLERMNTLLAG	3093
DYHC_YEAST	2778	GLKIVQPKIHRHNSLSDFDMLKKAISDCSLKESRTCLIIDESNILETAFLERMNTLLAN	2837
DYHC2_HUMAN	2733	GEVPGLYTLLEELPLLLPLKDAQSODGFF---GPVFNYFTYRIQQNLHIVLIMDSANSN	2788
DYHC_DICDI	3094	GEVPGLFEGEEFTALMHACKETAQRNGLILDSEELYKYFTSQVRRNLHVFTMNPASPD	3153
DYHC_YEAST	2838	ADIPDLFQGEEDKLLNLRNKRTRSLGLLDTEQELYDWFVGEIAKNLHVVTI CDPTNN	2897
DYHC2_HUMAN	2789	FMINCESNPALHKKCQVLWMEGWSNSMCKIPEMLFSETGG-GEKYNDKK-RKEEK----	2842
DYHC_DICDI	3154	FHNRSATSPALFNRCVLDWFGWSPALFQVGSEFTRNLDLENPQYIAPPVFIQAEIMG	3213
DYHC_YEAST	2898	KSSAMISSPALFNRCIINWMGDWDTKTMSQVANMVDVIPMEFTDFIVPEVNKELV--FT	2955
		AAA4S	
DYHC2_HUMAN	2843	-K----KNSVDPDFLKSFLLIH-----ESCKAYGATPSRYMTFLHVYSIAISSS	2885
DYHC_DICDI	3214	NNLMAIPPSHRDAVVSSLVYIHQTIQGEANIRLLKRQGRQNYVTPRHVLDYFINQVLLINE	3273
DYHC_YEAST	2956	EP----IQTIRDAVVNLIHFDRNFY-----QKMKVGVNPRSPGYFIDGLRALVKLVTA	3005
		Stalk CCI	

DYHC2_HUMAN	2886	KKKELLRQSHLQAGVSKLNEAKALVDELNRKAGEQSVLLKTKQDEADAALQMITVSMQD	2945
DYHC_DICDI	3274	KRDQLEEEQLHLNIGLKKLRDTEAQVKDLQVSLAQKNRELDVKNEQANQKQKQMVQDQQA	3333
DYHC_YEAST	3006	KYQDLQENQRFVNVGLEKLNESVLKVNELNKTLSKKSTELTEKEKEARSTLDKMLMEQNE	3065
		H8	
DYHC2_HUMAN	2946	ASEQKTELELERLKHRIAEEVVKIEERKNKIDDELKEVQPLVNEAKLAVGN IKPESLSEIRS	3005
DYHC_DICDI	3334	AEIKQKDARELQVQLDVRNKEIAVQVKVAYADLEKAEPALIEAQEAVSTIKKKHLDEIKS	3393
DYHC_YEAST	3066	SERKQEATEEIKKILKVQEEDIRKRKEVVMKSIQDIEPTILEAQRGVKNIKKQQLTEIRS	3125
		H8 → H1	
		MTBD	
DYHC2_HUMAN	3006	LRMPDPVIRDILEGVLRLMGIFDTSWVSMKSFLAKRGVREDIATFDARNIS-KEIRESVE	3064
DYHC_DICDI	3394	LPKPPTPVKLAMEAVCLMLGGKLEWADIRKKIMEFNFTSIIINYDTKKMTPKIREAIT	3453
DYHC_YEAST	3126	MVNPSPGVKIVMEAVCAILGYQFSNWRDIQQFIRKDDFIHNIVHYDTTLHMKPQIRKYME	3185
		H2 H3 H4 H5	
		Stalk CC2	
DYHC2_HUMAN	3065	ELLFKNKGSFDPKNAKRASTAAAPLAAWVKANIQYSHVLERIHPLETEQAGLESNLK TE	3124
DYHC_DICDI	3454	KG-YLEDPGFDYETVNRASKACGPLVKWATAQTYYSEILDRIKPLREEVEQLENAANELK	3512
DYHC_YEAST	3186	EE-FLSDPNFTYETINRASKACGPLYQWVNAQINFSKVLENVDPLRQEMKRIEFESLTKT	3244
		H5 H6 H9	
DYHC2_HUMAN	3125	DRKRKLEELLNSVGQKVSSELKEKFSRTSEAAKLEAEVSKAQETIKAAEVLINQLDREHK	3184
DYHC_DICDI	3513	LKQDEIVATITALEKSIATYKEEYATLIRETEQIKTESSKVNKVDRSIALLDNLNSERG	3572
DYHC_YEAST	3245	ANLLAAEEMTQDLEASIEVSKRKYSLIRDEVAIKTEMSNVQANLDRSISLVKSLTFEKE	3304
		H9	
DYHC2_HUMAN	3185	RWNAQVVEITEELATLPKRAQLAAAFITY LSAAPESLRKTCLEEWTKSAGLE-----KF	3238
DYHC_DICDI	3573	RWEQQSENFNTQMSTVVGDVVLSAFLAYIGFFDQNFRTDLMRKWMIRLDSVGIKFKSDL	3632
DYHC_YEAST	3305	RWLNTTKQFSKTSQELIGNCI ISSIYETYFGHLNERERADMLVILKRLLGKFAVKYDVNY	3364
		H9 H10	
DYHC2_HUMAN	3239	DLRRFLCTESEQLIWKSEGLPSDDLSENALVI-LQSRVCPFLIDPSSQATEWLKTHLKD	3297
DYHC_DICDI	3633	SVPSFLSKPEERLNWHANLPSDELCIENA-IMLKRFRNYPLVIDPSGQAMEFLMNQYAD	3691
DYHC_YEAST	3365	RFIDYLVTLDEKMKWLECGLDKNDYFLENMSIVMNSQDAVFFLLDPSSHMITVINSYYGN	3424
		H11 H0 S1 H1	
		AAA5L	
DYHC2_HUMAN	3298	SRLEVINQQDSNFITALELAVRFGKTLIIQEMDGVPEVLYPLL RRDLVAQGPRYVVQIGD	3357
DYHC_DICDI	3692	KKITKTSFLDSSF FMKNLES ALRFGCPLLVQDVENIDPVLNPNVFNKEIRKKGGRILIRLGD	3751
DYHC_YEAST	3425	-KTVLLSFL EEGFVKRLENAIRFGSVVVIQDGEFFDPIISRLISREFNHAGNRVTVEIGD	3483
		S2 H2 S3 H3	
DYHC2_HUMAN	3358	KIIDYNEEF RFLFLSTRNPNPFIPDAASIVTEVNF TT TRSGLRGQLLALTIQHEK PDLEE	3417
DYHC_DICDI	3752	QDVFSPSPFMI FLFTRDPTAHFTPDLC SRVTFVNF VTPTSSLQSQCLHEALKTERPDTHK	3811
DYHC_YEAST	3484	HEVDVSGDFKLF FIHSCDPSGDIPIFLRSRVLVH FVTN KESIETRIFDITLTEENAEMQR	3543
		S4 H4 S5 H5	
		AAA5S	
		Buttress CC1	
DYHC2_HUMAN	3418	QKTKLLQQEEDKKIQ LAKLEESLLET LAT SQGNILENKDLIESLNQTKASSALIQESLKE	3477
DYHC_DICDI	3812	KRSDLLKIQGEFQVKLRILEKSLNALSQASGNILDDDSVISTLETLKKETTEIALKVEE	3871
DYHC_YEAST	3544	KREDLILKLNTEYK LKLNLEKRLLEELNNSQGNMLENDELMTLNNLKKKEAMNIEKKLSE	3603
		Buttress CC2	
DYHC2_HUMAN	3478	SYKLQISLDQERDA YLP LAES ASKMYFII SDLS KINMYRFS LAA FLRFLQRALQNKQDS	3537
DYHC_DICDI	3872	TETVMQEISEVSALYNPMALSCSRVYFAMEELSQFHL-YQFSLRAFLDI FYN LLNNPNL	3930
DYHC_YEAST	3604	SEEFFPQFDNLVEEYS IIGKHSVKI F SMLEKFGQ FHW FGISIGQFLSCFKRVFIKKSRE	3663
		H6 H7	

DYHC2_HUMAN	3538	ENT-EQRIQSLI----SSLQHMVVEYICRCLFKADQLMFALHFV----RGMHPELFQENE	3588
DYHC_DICDI	3931	VD-KKDPNERLVYL-SKDI F SMTFNRVTRTLLNDDKLT FALQLTIISVKGTS-NEIEESE	3987
DYHC_YEAST	3664	TRAARTRVDEILWLLYQEVYC----QFSTAL--DKKFKMIMAMTMFCLYKF---DIESEQ	3714
DYHC2_HUMAN	3589	WDTFTGVVVGDMLRKADSQQKIRDQLPSWI----DQERSWAVATLKIALPSLYQ--TLCF	3642
DYHC_DICDI	3988	WDFLLK-----GGDNLTSIKETIPQLDSSLSTTQQKWLII-CLRQQVPSFSKLV DHIQ	4038
DYHC_YEAST	3175	Y-----KEAVLTMIGVLSSES-----SDGVPKLT--VDTNN	3742
DYHC2_HUMAN	3643	EDAALWRITYNNSMCE-----QEFPSILAKKVS L FQ Q I L V V Q A L R P D R L Q S A M	3690
DYHC_DICDI	4039	QNSSDWKQFFGKDQVGEPIIPESWIVAQAQLSNQQSTIVSNFRKILLMKA FHS DRVLQYS	4098
DYHC_YEAST	3743	DLRYLWDYVTTK---SYISALNWFK-----NEFFVD-----	3770
DYHC2_HUMAN	3691	ALFACKTLGLKEVSP L P L N L K R L Y K E T - L E I E P I L I I I S P G A D P S Q E L Q E L A N A E R S G E C	3749
DYHC_DICDI	4099	HSFVCSVFGEDFLNTQELDMANIVEKEVKSSSPLLCSVPGYDASSKVDDLALQL--HKQ	4156
DYHC_YEAST	3771	-----EWN I A D V V A N S E - - N N Y F T M A S E R D V D G T F K L I E L A K A S - - K E S	3810
DYHC2_HUMAN	3750	YHQVAMGQG-QADLAIQMLKECARNGDWLCLKNLHLVVS W L P V L E K E - - - - L N T L Q P K D T	3804
DYHC_DICDI	4157	YKSFAGSPEGFELAEKSIYAAAKSGTWLLKNIHLAPQWLVLQLEKK---LHSLSPHPS	4212
DYHC_YEAST	3811	LKIIPLGSIENLNYAQEEISKSKI EGGWILLQNIQMSLSWVKTYLHKHVEETKAAEEHEK	3870
DYHC2_HUMAN	3805	FRLWLTAEVH-PNFTPILLQSS L K I T Y E S P P G L K K N L M R T Y E S W T P E Q I S K K D N T H R A H A	3863
DYHC_DICDI	4213	FRLFMTSEIH-PALPANLLRMSNVFSYENPPGVKANLLHTFIGI-PATRMDKQPAERSRI	4270
DYHC_YEAST	3871	FKMFMTCHLTGDKLPAPLLQRTDRFVYEDIPGILDTVKDLWG-S-QFFTGKISGVWSVYC	3928
DYHC2_HUMAN	3864	LFSLAWFHAACQERRNYIPQGWTKFYEFSLSDLRAGYNIIDRLF-----DGAKDVQ	3914
DYHC_DICDI	4271	YFLLAWFHAIQERLRYIPLGWTKFEFNDADLRGALDSIDYWDVLYSKGRSNI DPDKIP	4330
DYHC_YEAST	3929	TFLLSWFHALITARTRLVPHGFSKKYFNDCCDFOFASVYLE-----NVLATNSTNNIP	3981
DYHC2_HUMAN	3915	WEFVHGLLENAIYGGRIDNYFDLRLVLSYLKQFFNSSVIDVFNQRNKKSI F P Y S V S L P Q S	3974
DYHC_DICDI	4331	WIAVRTILGSTIYGGRIDNEFDMRLLYS F L E Q L F T P S A F N P D F P - - - - L V - P S I G L S V P	4384
DYHC_YEAST	3982	WAQVRDHIATIVYGGKIDEEKDLEVVAKLCAHVFCGSDN---LQ-----IV-PGVRI PQP	4032
DYHC2_HUMAN	3975	-----C--SILDYRAVIEKIPEDDKPSFFGLPANIARSSQRMIS SQVISQLRILGRSI	4025
DYHC_DICDI	4385	-----EGTTRAHFMKW--IEALPEISTPIWLGLPENAESLLLSNKARKMINDLQKMQSSE	4437
DYHC_YEAST	4033	LLQQSEEEERARLTAI LSNTIEPADSLSSWLQLPRESILNYE-----RLOAKE	4080
DYHC2_HUMAN	4026	TAGSK-----FDREIWSNELSPVLNLWKKLNQNSNLIHQKVP P P N D R Q G S P	4071
DYHC_DICDI	4438	EDGEDDQVSGSSKKESSSSSEDK GKAKLRATIT E W T K L L P K P L Q - - - L K R T Q N I K D P	4494
DYHC_YEAST	4081	VASSTEQLLOEM-----	4092
DYHC2_HUMAN	4072	ILSFIILEQFNAIRLVQSVHQSLAALS K V I R G T T L L S S E V Q K L A S A L L N Q K C P L A W Q S K W	4131
DYHC_DICDI	4495	LFRCFEREISTGGKLVKKITNDLANLLELISGNIKSTNYLRSLTTSISKGIVPKEWK--W	4552
DYHC_YEAST			
DYHC2_HUMAN	4132	EGPEDPLQYLRLVARALAIQNWVDKAE-----KQALLSETLDLSELFHPDFTFL	4180
DYHC_DICDI	4553	YSVP-----ETISLSVWISDFSKRMQQLSEISESSDYSSIQVWLGGLLNPEAYI	4601
DYHC_YEAST			

DYHC2_HUMAN 4181 NALRQETARAVGRSVDLKFVASWKGRLQ-EAKLQIKISGLLLEGCSFDGNQLSENQLDS 4239
 DYHC_DICDI 4602 TATRQSASQLNGWSELENLRLHASLGLKISSSEGGASFNVKGMALLEGAVWNNNDQLTPTDILS 4661
 DYHC_YEAST



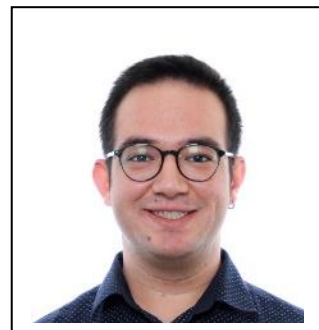
DYHC2_HUMAN 4240 PSVSSVLPFCFMGWIPQDACGPPSPDECISLPVYTSERDRVVTNIDVPCGGN--QDQWIQ 4297
 DYHC_DICDI 4662 TPIS---IATLTWKDKDDPIFNNSSSKLSVPVYLNTRSELFSIDLPHYDQSTSKQNWYQ 4718
 DYHC_YEAST



DYHC2_HUMAN 4298 CGAALFLKNQ-- 4307
 DYHC_DICDI 4719 RSVSISWKSIDI 4730
 DYHC_YEAST



CURRICULUM VITAE



Name Surname : Mert Gölcük

Place and Date of Birth : Adapazarı 18/07/1995

E-Mail : golcuk@itu.edu.tr

EDUCATION :

- **B.Sc.** : 2013-2018, Istanbul Technical University, Science and Letter, Molecular Biology and Genetics

OTHER PUBLICATIONS, PRESENTATIONS AND PATENTS:

1. Gur, M., **Golcuk, M.**, Yilmaz, S. Z., & Taka, E. (2019). Thermodynamic first law efficiency of membrane proteins. *Journal of Biomolecular Structure and Dynamics*, 1-11.
2. Gur, M., **Golcuk, M.**, Gul, A., & Erman, B. (2019). Molecular Dynamics Simulations Provide Molecular Insights into the Role of HLA-B51 in Behçet's Disease Pathogenesis. *Chemical Biology & Drug Design*. (Accepted).